P • A • R • T • 2

BIOMECHANICS OF THE HUMAN BODY

CHAPTER 4

FUNDAMENTAL CONCEPTS OF BIOHEAT TRANSFER AND RECENT APPLICATIONS USING HYPERTHERMIA IN CANCER TREATMENT

Liang Zhu
University of Maryland, Baltimore County, Baltimore, Maryland

4.1 INTRODUCTION 69
4.2 FUNDAMENTAL ASPECTS OF BIOHEAT TRANSFER 70
4.3 BIOHEAT TRANSFER MODELING 72
4.4 TEMPERATURE, THERMAL PROPERTY, AND BLOOD FLOW MEASUREMENTS 84
4.5 HYPERTHERMIA TREATMENT FOR CANCERS AND TUMORS 94
4.6 CONCLUSION 108
REFERENCES 108

4.1 INTRODUCTION

Over the past 100 years, the understanding of thermal and mechanical properties of human tissues and physics that governs biological processes has been greatly advanced by the utilization of fundamental engineering principles in the analysis of many heat and mass transport applications in biology and medicine. During the past two decades, there has been an increasingly intense interest in bioheat transfer phenomena, with particular emphasis on therapeutic and diagnostic applications. Relying on advanced computational techniques, the development of complex mathematical models has greatly enhanced our ability to analyze various types of bioheat transfer process. The collaborations among physiologists, clinicians, and engineers in the bioheat transfer field have resulted in improvements in prevention, treatment, preservation, and protection techniques for biological systems, including use of heat or cold treatments to destroy tumors or to improve patients' outcome after brain injury, and protection of humans from extreme environmental conditions.

Section 4.2 starts with fundamental aspects of thermal interaction between blood and its surrounding tissue. Discussions on how thermal effect of blood is modeled in biological systems then follow in Sec. 4.3. Section 4.4 shows different approaches for theoretically modeling the blood flow in the tissue. In particular the assumptions and validity of several widely used continuum bioheat transfer equations are evaluated. Different techniques to measure temperature, thermophysical properties, and blood flow in biological systems are described in Sec. 4.5. Section 4.6 focuses on one of the medical applications of heat transfer, hyperthermia treatment for tumors, with emphases on traditional and current heating techniques and advanced modeling approaches.

ch04.indd 69 16-11-2020 17:35:08

4.2 FUNDAMENTAL ASPECTS OF BIOHEAT TRANSFER

One of the remarkable features of the human thermoregulatory system is that we can maintain a core temperature near 37°C over a wide range of environmental conditions and during thermal stress. The value of blood flow to the body varies over a wide range depending upon the need for its three primary functions:

1. *Mass transfer in support of body metabolisms:* Blood transports oxygen to the rest of the body and transports carbon dioxide and other waste from the cells.
2. *Regulation of systemic blood pressure:* The vascular system is a primary effector in the regulation of systemic blood pressure through its ability to alter the distribution of blood flow and regulate the cardiac output and thereby buffer systemic pressure fluctuations.
3. *Heat transfer for systemic thermoregulation***.**

As for the last primary function, blood is known to have a dual influence on the thermal energy balance. First, it can be a heat source or sink, depending on the local tissue temperature. During winter time, blood is transported from the heart to warm the rest of the body. On the other hand, during hyperthermia treatment for certain diseases where tissue temperature is elevated to as high as 45°C by external devices, relatively cold blood forms cold tracks that can decrease the treatment efficacy. The second influence of blood flow is that it can enhance heat dissipation from the inside of the body to the environment to maintain a normal body temperature. Theoretical studies have shown that if the heat produced in the central areas of the body at rest condition could escape only by tissue conduction, the body temperature would not reach a steady state until it was about 80°C. A lethal temperature would be reached in only 3 hours. During exercise, our body temperature would have typically risen 12°C in 1 hour if no heat were lost by blood flow. Maintaining a core temperature of 37°C during thermal stress or exercise in the body is achieved by increasing the cardiac output by central and local thermoregulation, redistributing heat via the blood flow from the muscle tissue to the skin, and speeding the heat loss to the environment by evaporation of sweat.

Thermal interaction between blood and tissue can be studied either experimentally or theoretically. However, for the following reasons it is difficult to evaluate heat transfer in a biological system:

- *The complexity of the vasculature:* It is not practical to develop a comprehensive model that includes the effect of all thermally significant vessels in a tissue. Therefore, the most unusual and difficult basic problem of estimating heat transfer in living biologic systems is modeling the effect of blood circulation.
- *Temperature response of the vasculature to external and internal effects:* It is also a complex task. In a living system, the blood flow rate and the vessel size may change as a response to local temperature, local pH value, and the concentration of local O_2 and CO_2 levels.
- *The small thermal length scale involved in the microvasculature:* Thermally significant blood vessels are generally in a thermal scale of less than 300 μm. It has been difficult to build temperature-measuring devices with sufficient resolution to measure temperature fluctuation.

For the above reasons, even if the heat transfer function of the vascular system has been appreciated since the mid-nineteenth century, only in the past four decades, has there been a revolution in our understanding on how temperature is controlled at the local level, i.e., how local microvascular blood flow controls the local temperature field and how the local tissue temperature regulates local blood flow.

Until 1980, it was believed that, like gaseous transport, heat transfer took place in the capillaries because of their large exchange surface area. Several theoretical and experimental studies (Chato, 1980; Chen and Holmes, 1980; Lemons et al., 1987; Weinbaum et al., 1984) have been performed to illustrate how individual vessels participate in local heat transfer and thus to understand where the actual heat transfer between blood and tissue occurs. Since heat transfer requires temperature difference, it is essential to identify blood vessels where their temperatures are higher or lower

than the temperature of their surrounding tissue. In these analyses, the concept of thermal equilibration length was introduced. Thermal equilibration length of an individual blood vessel was defined as a distance over which the temperature difference between blood and tissue drops a certain percentage. For example, the axial variation of the tissue and blood temperature difference can be expressed as $\Delta T = \Delta T_0 e^{-\frac{x}{x_{cr}}}$, where ΔT_0 is the temperature difference at the vessel entrance, and x_{cr} and $4.6x_{cr}$ are the thermal equilibration length over which ΔT decreases to 37 percent and 1 percent, respectively, of its value at the entrance. A blood vessel whose thermal equilibration length is comparable to its physical length L is considered thermally significant, and thus, its thermal effect on tissue temperature field should be included in theoretical modeling. If the thermal equilibration length is much longer than the physical length, the blood temperature changes very little along its length. However, when the thermal equilibration length is much shorter than L, the blood temperature along the vessel should be very close to the local tissue temperature, and thus, the thermal effect of those blood vessels can often be neglected in theoretical modeling.

Chato (1980) first theoretically investigated the heat transfer from individual blood vessels in three configurations: a single vessel, two vessels in countercurrent flow, and a single vessel near the skin surface. It was shown that the Graetz number, proportional to the blood flow velocity and radius, is the controlling parameter determining the thermal equilibration between the blood and tissue. For blood vessels with very low Graetz number, blood quickly reaches the tissue temperature. It was also demonstrated that heat transfer between the countercurrent artery and vein is affected by the vessel center-to-center spacing and mass flow rate between them.

In an anatomic study performed on rabbit limbs, Weinbaum et al. (1984) identified three vascular layers (deep, intermediate, and cutaneous) in the outer 1-cm tissue layer. Subsequently, three fundamental vascular structures were derived from the anatomic observation: (1) an isolated vessel embedded in a tissue cylinder, as shown by the intermediate tissue layer; (2) a large artery and its countercurrent vein oriented obliquely to the skin surface, as shown in the deep tissue layer; and (3) a vessel or vessel pair running parallel to the skin surface in the cutaneous plexus. These three vascular structures served as the basic heat transfer units in the thermal equilibration analysis in Weinbaum et al. (1984).

As shown in Weinbaum et al. (1984), 99 percent thermal equilibration length of a single blood vessel embedded in a tissue cylinder was derived as

$$x_{cr} = 1.15 * a * \mathrm{Pr} * \mathrm{Re}_D [0.75 + K * \ln(R/a)] \tag{4.1}$$

where a and R are the blood vessel and tissue cylinder radius, respectively, Pr and Re_D are the blood flow Prandtl number and Reynolds number, respectively, and K is the ratio of blood thermal conductivity to tissue thermal conductivity. It is evident that x_{cr} is proportional to the blood vessel size and its blood flow velocity. Substituting the measured vascular geometry and the corresponding blood flow rate number for different blood vessel generations (sizes) from a 13-kg dog (Whitmore, 1968), one could calculate the thermal equilibration length as listed in Table 4.1.

Several conclusions were drawn from the comparison between x_{cr} and L. In contrast to previous assumptions that heat transfer occurs in the capillary bed, for blood vessels smaller than 50 μm in diameter, blood temperature quickly reaches the tissue temperature; thus, all blood-tissue heat transfer must have already occurred before entering into these vessels. For blood vessels larger than 300 μm in diameter, there is little change in blood temperature in the axial direction because of their much longer thermal equilibration length compared with the vessel length. The medium-sized vessels between 50 and 300 μm in diameter are considered thermally significant because of their comparable thermal equilibration length and physical length. Those blood vessels are primary contributors to tissue heat transfer. Note that the conclusions are similar to that drawn by Chato (1980).

It was observed that virtually all the thermally significant vessels (>50 μm in diameter) in the skeletal muscle were closely juxtaposed artery-vein pairs (Weinbaum et al., 1984). The countercurrent heat exchange mechanism, if dominant, was suggested as an energy conservation means since it provides a direct heat transfer path between the vessels. Therefore, it leads to a small thermal resistance between the warm artery and its countercurrent vein. Thermal equilibration in the artery

TABLE 4.1 Thermal equilibration length in a single vessel embedded in a tissue cylinder

Vessel radius a, μm	Vessel physical length L, cm	R/a	x_{cr}, cm
300	1.0	30	9.5
100	0.5	20	0.207
50	0.2	10	0.014
20	0.1	7	0.0006

(50~300 μm in diameter) in a countercurrent pair was estimated based on a simple heat conduction analysis in the cross-sectional plane. It was noted that the thermal equilibration length in the countercurrent artery was at least three times shorter than that in a single vessel of the same size embedded in a tissue cylinder (Weinbaum et al., 1984). A short thermal equilibration length indicates a smaller thermal resistance due to the short cut of heat transfer pathway between the countercurrent artery and vein. Significantly short thermal equilibration length in comparison with that of a single vessel suggests that the primary blood tissue heat exchange mechanism for vessels larger than 50 μm in the deep layer is the incomplete countercurrent heat exchange. Therefore, for modeling heat transfer in these tissue regions, reasonable assumptions related to the countercurrent heat exchange mechanism can be made to simplify the mathematical formulation.

Theoretical analyses of the thermal equilibration in a large vessel in the cutaneous layer (Chato, 1980; Weinbaum et al., 1984) demonstrated that its thermal equilibration length was much longer than its physical length during normal and hyperemic conditions despite the close distance from the skin surface. It was suggested that the large vessels in the cutaneous layer can be far from thermal equilibration and are therefore capable of delivering warm blood from the deep tissue to the skin layer. This superficial warm blood shunting is very important in increasing the normal temperature gradient at the skin surface and therefore plays an important role in losing heat during heavy exercise. On the contrary, during surface cooling there is rapid cutaneous vasoconstriction in the skin. The minimally perfused skin, along with the underlying subcutaneous fat, provides a layer of insulation, and the temperature gradient from the skin surface into the muscle becomes almost linear (Bazett, 1941) yielding the lowest possible heat transfer from the body.

4.3 BIOHEAT TRANSFER MODELING

The effects of blood flow on heat transfer in living tissue have been examined for more than a century, dating back to the experimental studies of Bernard in 1876. Since then, mathematical modeling of the complex thermal interaction between the vasculature and tissue has been a topic of interest for numerous physiologists, physicians, and engineers. A major difficulty to theoretically predict temperature distribution in tissue is the assessment of the thermal effect of blood circulation, which is the dominant mode of heat removal or release and is an important cause of tissue temperature inhomogeneity.

Because of the complexity of the vascular geometry, there are two theoretical approaches describing the effect of blood flow in a biological system. Each approach represents two length scales over which temperature variations may occur.

1. *Continuum models,* in which the effect of blood flow in the region of interest is averaged over a control volume. Thus, in the considered tissue region, there is no blood vessel present; however, its effect is treated by either adding an additional term in the conduction equation for the tissue or changing some of the thermal/physical parameters in the conduction equation. The continuum

models are simple to use since the detailed vascular geometry of the considered tissue region need not be known as long as one or two representative parameters related to the blood flow are available. The shortcoming of the continuum model is that since the blood vessels disappear, no point-by-point variation in the blood temperature is available. Another shortcoming is associated with the assumptions introduced when the continuum model was derived. For different tissue regions and physiological conditions, these assumptions may not be valid.

2. *Vascular models,* in which blood vessels are represented as tubes buried in tissue. Because of the complicated vascular geometry one may only consider several blood vessels and neglect the others. Previous studies (Crezee and Lagendijk, 1990; Dorr and Hynynen, 1992; Roemer, 1990; Wang and Zhu, 2007; Wang et al., 2008) have demonstrated that blood flow in large, thermally unequilibrated vessels is the main cause for temperature nonhomogeneity during hyperthermia treatment. Large blood vessels may significantly cool tissue volumes around them, making it very difficult to cover the whole tumor volume with therapeutic thermal exposure. In applications where point-to-point temperature nonuniformities are important, vascular model has been proved to be necessary to predict accurately the tissue temperature field (Wang and Zhu, 2007; Zhu et al., 1996a). In recent years, with the breakthrough of advanced computational techniques and resources, vascular models (Raaymakers et al., 2000) for simulating vascular networks have grown rapidly and already demonstrated its great potential in accurate and point-to-point blood and tissue temperature mapping.

4.3.1 Continuum Models

In continuum models, blood vessels are not modeled individually. Instead, the traditional heat conduction equation for the tissue region is modified by either adding an additional term or altering some of the key parameters. The modification is relatively simple and is closely related to the local vasculature and blood perfusion. Even if the continuum models cannot describe the point-by-point temperature variations in the vicinity of larger blood vessels, they are easy to use and allow the manipulation of one or several free parameters. Thus, they have much wider applications than the vascular models. In the following sections, some of the widely used continuum models are introduced and their validity is evaluated on the basis of the fundamental heat transfer aspects.

Pennes Bioheat Equation. It is known that one of the primary functions of blood flow in a biological system is their ability to heat or cool the tissue, depending on the relative local tissue temperature. The existence of a temperature difference between the blood and tissue is taken as evidence of its function to remove or release heat. On the basis of this speculation, Pennes (1948) proposed his famous heat transfer model, which is called Pennes bioheat equation. Pennes suggested that the effect of blood flow in the tissue be modeled as a heat source or sink term added to the traditional heat conduction equation. The Pennes bioheat equation is given by

$$\rho_t c_t \frac{\partial T_t}{\partial t} = k_t \nabla^2 T_t + q'''_{\text{blood}} + q'''_m \tag{4.2}$$

where q'''_m is the volumetric metabolic heat generation rate in the tissue, and the second term on the right side of the equation (q'''_{blood}) takes into account the contribution of blood flow to the local tissue temperature distribution. The strength of the perfusion source term can be derived as follows.

Figure 4.1 shows a schematic diagram of a small tissue volume perfused by a single artery and vein pair. The tissue region is perfused via a capillary network bifurcating from the transverse arterioles, and the blood is drained by the transverse venules. The blood flow rate in the supply artery decreases while that in the supply vein increases. Mass conservation requires that the amount of the blood flow rate change in the supply artery or vein is the same, i.e.,

$$Q_{\text{in},a} - Q_{\text{out},a} = Q_{\text{out},v} - Q_{\text{in},v} = \Delta Q_{O_2-CO_2} \tag{4.3}$$

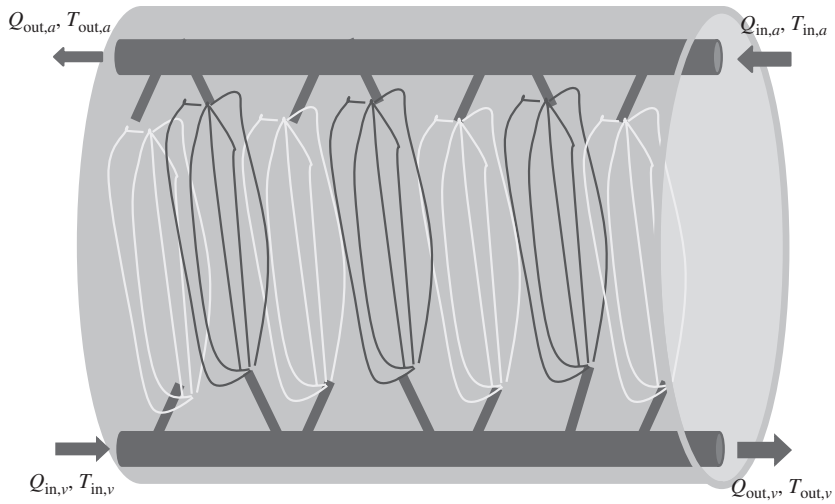

FIGURE 4.1 Schematic diagram of a tissue volume perfused by a single artery and vein pair.

If one assumes that both the artery and vein keep a constant temperature when they pass through this tissue region, the total heat released is equal to the total amount of blood perfusing this tissue volume per unit time, $\Delta Q_{O_2-CO_2}$, multiplied by its density ρ_b, specific heat c_b, and the temperature difference between the artery and vein, and is given by

$$\rho_b c_b \Delta Q_{O_2-CO_2}(T_a - T_v) \qquad (\mathrm{W}) \tag{4.4}$$

The volumetric heat generation rate q'''_{blood}, defined as the heat generation rate per unit tissue volume V, is then derived as

$$q'''_{blood} = \frac{\rho_b c_b \Delta Q_{O_2-CO_2}(T_a - T_v)}{V} = \frac{\Delta Q_{O_2-CO_2}}{V}\rho_b c_b (T_a - T_v) = \omega \rho_b c_b (T_a - T_v) \qquad \left(\frac{\mathrm{W}}{\mathrm{mL}}\ or\ \frac{\mathrm{W}}{\mathrm{m}^3}\right) \tag{4.5}$$

where ω is defined as the amount of blood perfused per unit volume tissue per second and it is given by the following equation:

$$\omega = \Delta Q_{O_2-CO_2}/V \qquad \left(\frac{1}{\mathrm{s}}\right) \tag{4.6}$$

Notice the slight difference of the unit in Eq. (4.6) for the blood perfusion rate from the one in medical literature, where the blood perfusion rate usually carries a unit of mL/g tissue*s. When the density of tissue is known, one should be able to convert it from the value given in medical literature to the one defined in Eq. (4.6).

Both T_a and T_v in Eq. (4.5) are unknown. Applying the analogy with gaseous exchange in living tissue, Pennes believed that heat transfer occurred in the capillaries because of their large area for heat exchange. As shown in Fig. 4.2, Pennes stated that the local arterial temperature T_a could be assumed as a constant and equal to the artery blood temperature from the heart, T_{b0}. As for the local venous blood, it seems reasonable to assume that it equilibrates with the tissue in the capillary, and when the blood enters the venules from the capillary, it has a similar temperature as the local tissue temperature. Figure 4.2 also illustrates that when the countercurrent heat exchange between the paired large artery and vein is neglected, the temperature of the venous blood in systemic circulation

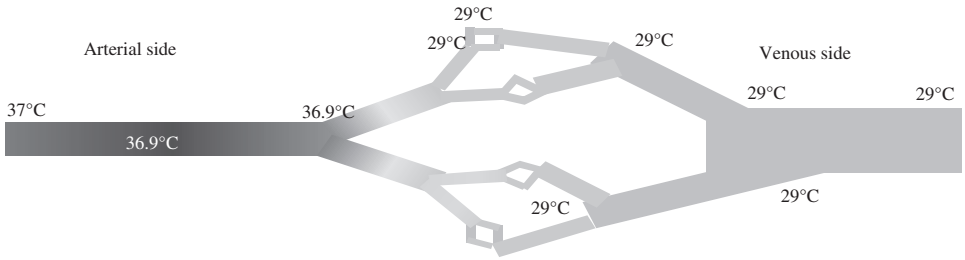

FIGURE 4.2 Schematic diagram of temperature variations in the vasculature and its surrounding tissue assumed by Dr. Pennes.

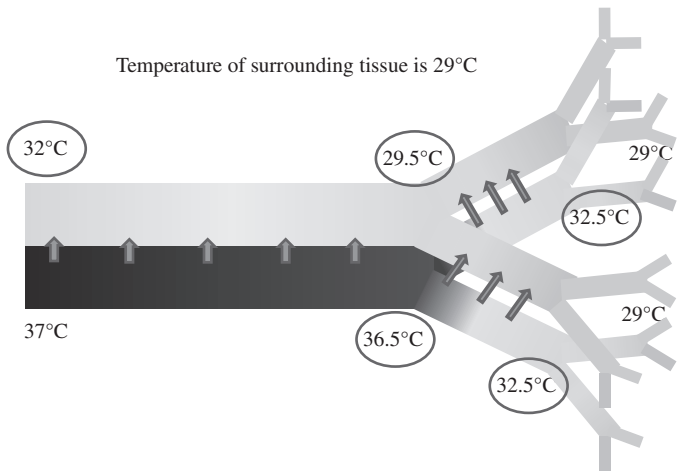

FIGURE 4.3 Schematic diagram of realistic temperature variations in the vasculature and its surrounding tissue considering heat exchange between blood and tissue, as well as between countercurrent artery and vein.

T_v would remain the same as its surrounding tissue temperature T_t. Then, the Pennes bioheat equation becomes

$$\rho_t c_t \frac{\partial T_t}{\partial t} = k_t \nabla^2 T_t + \omega \rho_b c_b (T_{b0} - T_t) + q_m''' \tag{4.7}$$

This is a partial differential equation for the tissue temperature field, when T_{b0} is often prescribed as 37°C. As long as an appropriate initial condition and boundary conditions are prescribed, the transient or steady-state temperature field in the tissue can be determined.

The limitations of the Pennes equation come from the basic assumptions introduced in this model. First, it is assumed that the temperature of the arterial blood does not change when it travels from the heart to the capillary bed. As shown in Fig. 4.3, small temperature variations occur only in blood vessels with a diameter larger than 300 μm. Another assumption is that the venous blood temperature is approximated by the local tissue temperature. This is valid only for blood vessels with a diameter smaller than 50 μm. Thus, without considering the thermal exchange between the countercurrent artery and vein in different vessel generations, the Pennes perfusion source term obviously overestimates the effect of blood perfusion. To accurately model the effect of blood perfusion, the temperature variation along the artery and the heat recaptured by the countercurrent vein must be taken into consideration.

Despite the limitations of the Pennes bioheat equation, reasonable agreement between theory and experiment has been obtained for the measured temperature profiles in perfused tissue subject to

various heating protocols. This equation is relatively easy to use, and it allows the manipulation of two blood-related parameters, the volumetric perfusion rate and the local arterial temperature, to modify the results. Pennes performed a series of experimental studies to validate his model. Over the years, the validity of the Pennes bioheat equation has been largely based on macroscopic thermal clearance measurements in which the adjustable free parameter in the theory, the blood perfusion rate (Xu and Anderson, 1999), was chosen to provide a reasonable agreement with experiments for the temperature decay in the vicinity of a thermistor bead probe. Indeed, if the limitation of Pennes bioheat equation is an inaccurate estimation of the strength of the perfusion source term, an adjustable blood perfusion rate will overcome its limitations and provide a reasonable agreement between experiment and theory.

Weinbaum-Jiji Bioheat Equation. Since 1980, researchers (Chato, 1980; Chen and Holmes, 1980; Weinbaum et al., 1984) have begun to question the validity of the Pennes bioheat equation. Later, Weinbaum and Jiji (1985) developed a new equation for microvascular blood tissue heat transfer, based on an anatomic analysis (Weinbaum et al., 1984) to illustrate that the predominant mode of heat transfer in the tissue was the countercurrent heat exchange between a thermally significant artery and vein pair. The near-perfect countercurrent heat exchange mechanism implies that most of the heat leaving the artery is transferred to its countercurrent vein rather than released to the surrounding tissue. Once there is a tissue temperature gradient along the countercurrent vessel axes, the artery and vein will transfer a different amount of energy across a plane perpendicular to their axes even if there is no net mass flow. This gives rise to a net energy transfer that is equivalent to an enhancement in tissue conductivity in the axial direction of the vessels. In the Weinbaum-Jiji bioheat equation, the thermal effect of the blood perfusion is described by an enhancement in thermal conductivity k_{eff}, appearing in the traditional heat conduction equation,

$$\rho_t c_t \frac{\partial T_t}{\partial t} = k_{\text{eff}} \nabla^2 T_t + q_m''' \qquad k_{\text{eff}} = k_t\left[1 + f(\omega)\right] \tag{4.8}$$

It was shown that k_{eff} is a function of the local blood perfusion rate and local vascular geometry.

The main limitations of the Weinbaum-Jiji bioheat equation are associated with the importance of the countercurrent heat exchange. It was derived to describe heat transfer in peripheral tissue only, where its fundamental assumptions are most applicable. In tissue area containing big blood vessels (>200 μm in diameter), the assumption that most of the heat leaving the artery is recaptured by its countercurrent vein could be violated; thus, it is not an accurate model to predict the temperature field. In addition, this theory was primarily developed for closely paired microvessels in muscle tissue, which may not always be the main vascular structure in other tissues, such as the renal cortex. Furthermore, unlike the Pennes bioheat equation, which requires only the value of local blood perfusion rate, the estimation of the enhancement in thermal conductivity requires that detailed anatomical studies be performed to estimate the vessel number density, size, and artery-vein spacing for each vessel generation, as well as the blood perfusion rate (Zhu et al., 1995). These anatomic data are normally not available for most blood vessels in the thermally significant range.

A New Modified Bioheat Equation. The Pennes and Weinbaum-Jiji models represent two extreme situations of blood-vessel thermal interaction. In the original Pennes model, the arterial blood releases all of its heat to the surrounding tissue in the capillaries and there is no venous rewarming. Pennes did not realize that thermal equilibration was achieved in vessels at least an order of magnitude larger than the capillaries. In contrast, in the Weinbaum-Jiji model the partial countercurrent rewarming is assumed to be the main mechanism for blood-tissue heat transfer. The derivation of the Weinbaum-Jiji equation is based on the assumption that heat transfer between the artery and the vein does not depart significantly from a perfect countercurrent heat exchanger. In other words, most of the heat lost by the artery is recaptured by its countercurrent vein rather than lost to the surrounding tissue. Subsequent theoretical and experimental studies have shown that this is a valid assumption only for vessels less than 200 μm diameter (Charny et al., 1990; Zhu et al., 1996a).

Several theoretical studies have suggested that one way to overcome the shortcomings of both models was to introduce a "correction coefficient" in the Pennes perfusion term (Baish, 1994; Brinck and Werner, 1994; Chato, 1980; Weinbaum et al., 1997; Zhu et al., 2002). In 1997, Weinbaum and

coworkers (Weinbaum et al., 1997) modified the Pennes source term on the basis of the thermal analysis of a basic heat transfer unit of muscle tissue, a 1-mm-diameter tissue cylinder containing blood vessels smaller than 200 μm in diameter, as shown in Fig. 4.4. The countercurrent heat exchange between the *s* artery and vein defined in the anatomical studies of Myrhage and Eriksson (1984) led to the estimation of the heat loss recaptured by the *s* vein. The strength of the source term was then rederived taking into account the rewarming of the countercurrent venous blood in the *s* tissue cylinder. The thermal equilibration analysis on the countercurrent *s* artery and vein in the tissue cylinder led to the following bioheat transfer equation:

$$\rho_t c_t \frac{\partial T_t}{\partial t} = k_t \nabla^2 T_t + \varepsilon \omega \rho_b c_b (T_{a0} - T_t) + q_m''' \tag{4.9}$$

Note that the only modification to the Pennes model is a correction coefficient ε in the Pennes perfusion source term. This correction coefficient can be viewed as a weighting function to correct the overestimation of the original Pennes perfusion term. An easy-to-use closed-form analytic expression was derived for this coefficient that depends on the vessel spacing and radius. From the anatomic studies of the vascular arrangements of various skeletal muscles, the correction coefficient was found to vary from 0.6 to 0.8 under normal physiological conditions, indicating that there is a 20 to 40 percent rewarming of the countercurrent vein. Similarly, one early work (Baish, 1994) was based on a generated vascular network following diffusion of angiogenic factors in tissue and it has shown that the Pennes perfusion source term overestimates the strength of heat released to or absorbed by the local blood perfusion by approximately 20 percent, implying a correction coefficient of 0.8. Note that it is close to neither unity (the Pennes model) nor zero (the Weinbaum-Jiji model). Thus, both the Pennes and Weinbaum-Jiji bioheat equations are not valid for most muscle tissue. The accuracy of

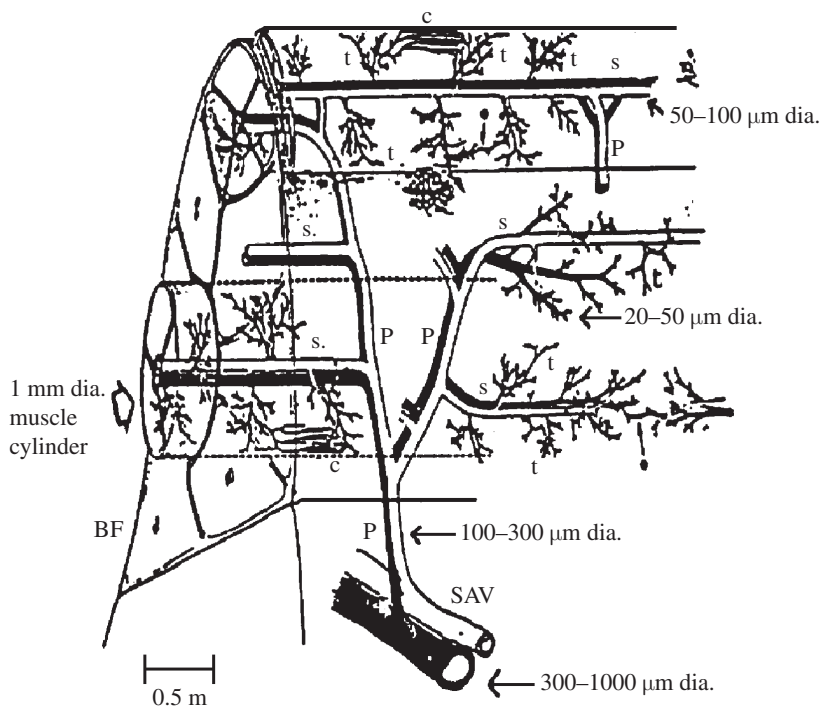

FIGURE 4.4 Macro- and microvascular arrangement in skeletal muscle. The blood supply for the muscle tissue cylinder comes from a branching countercurrent network of supply vessels. The primary (*P*) vessels originating from the *SAV* vessels run obliquely across the muscle tissue cylinders and then branch into the long secondary (*s*) vessels. [*From Myrhage and Erriksson (1984) with permission.*]

the calculated correction coefficients in the previous studies still depends on the precise description of the local vasculature arrangements and whether a repeatable tissue unit can be identified in the targeted tissue region. Unfortunately, in tissue region such as tumors, the blood flow patterns are often irregular and unpredictable, making the derivation of the correction coefficient a difficult task. Furthermore, as shown in Zhu et al. (2002), the arterial temperature T_{a0} may not be approximated as a constant either, unless the local blood perfusion is very high. In most physiological conditions, it is a function of the tissue depth, blood vessel bifurcation pattern, and the local blood perfusion rate.

Current Status of Bioheat Transfer Modeling. There were only a few attempts to develop alternative bioheat transfer models in the past 10 years based on volume averaging temperatures of porous media (Nakayama and Kuwahara, 2008; Shrivastava and Vaughan, 2009). One thing that is not clear from those models is the calculation of the "to-be-determined" parameters appearing in those equations. The determination of those parameters still requires development of a vasculature-tissue unit for establishing their relationship to the specific vasculature and blood perfusion rate.

Although developments of new bioheat transfer models have attracted a lot of attention in the 1980s and 1990s, most of the developed bioheat models have not yet been applied regularly by bioengineering researchers due to the uncertainty of estimating the parameters such as the enhancement in tissue thermal conductivity and the correction coefficient. The Pennes bioheat equation, utilizing only local perfusion rate and arterial blood temperature, is relatively easy to use without detailed anatomic knowledge of their detailed vasculature. In the past 10 years, very limited efforts have been focused on developing a better bioheat transfer models, with a few exceptions (Nakayama and Kuwahara, 2008; Shrivastava and Vaughan, 2009). Currently, the thermal effects of small blood vessels are still normally modeled by the Pennes perfusion source term, with special treatments to the large vessels. The emphases of bioheat transfer modeling have been shifted to model large individual blood vessels and its thermal interaction with the detailed anatomic geometry in the tissue region. This is largely due to the advancements in computational resources which allow import of three-dimensional tissue geometry from MRI or CT imaging systems to commercially available numerical simulation software packages. The dramatic increase in computer memory and calculating speed in the past decade enables the simulation of both steady state and transient temperature distribution in three-dimensional tissue structures with embedded individual large blood vessels.

4.3.2 Experimental and Theoretical Studies to Validate the Models

Pennes (1948) performed a series of experimental studies to validate his model. He inserted and pulled thermocouples through the arms of nine male subjects to measure the radial temperature profiles. He also measured the skin temperature distributions along the axis of the upper limb, as well as around the circumference of the forearm. Pennes then modeled the arm as a long cylinder and calculated the steady-state radial temperature profile. In this theoretical prediction, since the blood perfusion rate ω could not be directly measured, Pennes adjusted this parameter in his model to fit the solution to his experimental data for a fixed, representative ambient temperature and metabolic heating rate. The fitted value of blood perfusion rate ω was found to be between 1.2 and 1.8 mL blood/min/100 g tissue, which is a typical range of values for resting human skeletal muscle. Wissler (1998) reevaluated Pennes' original paper and analyzed his data. He found that the theoretical prediction agrees very well with Pennes' experimental results if the data were analyzed in a more rigorous manner.

Profound understanding of the heat transfer site and the countercurrent heat exchange between paired significant vessels was gained through previous experiments (Lemons et al., 1987) performed on rabbit thigh to measure the transverse tissue temperature profiles in the rabbit thigh using fine thermocouples. The experimental study was designed to achieve two objectives. The first is to examine whether there exists detectable temperature difference between tissue and blood for different-size vessels. Existing detectable blood-tissue temperature difference implies that blood has not established thermal equilibration with its surrounding tissue. The second is to examine the temperature difference between the countercurrent artery and vein. If the countercurrent heat exchange is dominant in blood tissue heat transfer, the vein must recapture most of the heat leaving the artery; thus, the venous blood would have a temperature significantly higher than the surrounding tissue

temperature. Using thermocouples to mapping temperature profiles in tissue, Lemons et al. (1987) performed in vivo experiments and considered local temperature bumps along the temperature profile as indications of existence of a warmer artery or vein nearby.

Experimental measurements by Lemons et al. (1987) recorded small temperature bumps of up to 0.5°C along the tissue path in the deep tissue region. The irregularities in the tissue temperature profiles were closely associated with the existence of blood vessels in the vicinity of the thermocouple wire. It was shown that temperature fluctuation was observed in all the blood vessels larger than 500 μm, in 67 percent of the vessels between 300 and 500 μm, and in 9 percent of the vessels between 100 and 300 μm. No temperature bump was observed in blood vessels less than 100 μm in diameter. This finding indicates that the assumption in the Pennes model that arterial blood reaches the capillary without significant prior thermal equilibration is inaccurate for this vascular architecture, and thus most of the significant blood-tissue heat transfer occurs in the larger vessels upstream. It was also observed that the temperature field near a large countercurrent artery and vein pair showed two temperature bumps rather than one temperature bump. This implies that the venous blood in the vein receives heat from its warm countercurrent artery nearly; thus, the temperature of the venous blood is raised close to the arterial blood temperature, rather than close to the local tissue temperature, as illustrated in the schematic diagram in Fig. 4.3.

Similar experiments were performed by He et al. (2002, 2003) to measure directly the temperature decays along the femoral arteries and veins and their subsequent branches in rats, using thermocouples attached to the surfaces of countercurrent artery and vein pairs of difference vessel generations. The experimental results have demonstrated that the venous blood in mid-size blood veins recaptured up to 41 percent of the total heat released from their countercurrent arteries under normal conditions. As expected, the contribution of countercurrent rewarming is reduced significantly to less than 15 percent for hyperemic conditions.

In a series of experiments with an isolated perfused bovine kidney, Crezee and Lagendijk (1990) inserted a small plastic tube into the tissue of a preserved bovine kidney and measured the resulting temperature fields in a plane perpendicular to the tube while heated water was circulated through it, with the kidney cortex perfused at different perfusion rates. They also used thermocouples to map the temperature distribution in the tissue of isolated bovine tongues perfused at various perfusion rates (Crezee et al., 1991). By examining the effect of increased perfusion on the amplitude and width of the thermal profile, they demonstrated that the temperature measurements agreed better with a perfusion-enhanced k_{eff} as opposed to the perfusion source term in the Pennes equation.

Charny et al. (1990) developed a detailed one-dimensional (1D) three-equation model. Since this model was based on energy conservation and no other assumptions were introduced to simplify the analysis of the blood flow effect, it was viewed as a relatively more accurate model than both the Pennes and Weinbaum-Jiji equation. The validity of the assumptions inherent in the formulation of the Weinbaum-Jiji equation was tested numerically under different physiological conditions. In addition, the temperature profile predicted by the Pennes model was compared with that by the three-equation model and the difference between them was evaluated. The numerical simulation of the axial temperature distribution in the limb showed that the Weinbaum-Jiji bioheat equation provided very good agreement with the three-equation model for downstream vascular generations that are located in the outer layer in the limb muscle, while the Pennes model yielded better description of heat transfer in the upstream vessel generations. Considering that vessels bifurcate from approximately 1000 μm in the first generation to 150 μm in the last generation, one finds that the Pennes source term, which was originally intended to represent an isotropic heat source in the capillaries, is shown to describe instead the heat transfer from the largest countercurrent vessels, more than 500 μm in diameter. The authors concluded that this was largely attributed to the capillary bleed-off from the large vessels in these tissue regions. The capillary bleed-off appeared to result in a heat source type of behavior that matches the Pennes perfusion term. The Weinbaum-Jiji model, on the other hand, significantly overestimated the countercurrent heat exchange in the tissue region containing larger blood vessels. The validity of the Weinbaum-Jiji equation requires that the ratio of the thermal equilibration length L_e of the blood vessel to its physical length L be less than 0.2. This criterion was found to be satisfied for blood vessels less than 300 μm in diameter under normothermic conditions.

4.3.3 Heat Transfer Models of the Whole Body

As outlined above, due to the complexity of the vasculature, continuum models appear more favorable in simulating the temperature field of the human body. In the Pennes bioheat equation, blood temperature is considered to be the same as the body core temperature or the arterial temperature at the heart; in the Weinbaum-Jiji bioheat equation, on the other hand, the effect of the blood temperature serves as the boundary condition of the simulated tissue domain. In either continuum model (Pennes or Weinbaum-Jiji), blood temperature is an input to the governing equation of the tissue temperature. However, in situations in which the blood temperature is actively lowered or elevated, both continuum models seem inadequate to account for the tissue-blood thermal interactions and to accurately predict the expected body temperature changes.

The human body has limited ability to maintain a normal, or euthermic, body temperature. The vasculature facilitates the redistribution and transfer of heat throughout the body preserving a steady core temperature for all vital organs and making the human body relatively insensitive to environmental temperature changes. In extreme situation such as heavy exercise or harsh thermal environment, the body temperature can shift to a high or low level from the normal range. Active control of body temperature is increasingly employed therapeutically in several clinical scenarios, most commonly to protect the brain from the consequences of either primary (i.e., head trauma, stroke) or secondary injury (i.e., after cardiac arrest with brain hypoperfusion). Mild to moderate hypothermia, during which brain temperature is reduced to 30 to 35°C, has been studied, among others, as an adjunct treatment for protection from cerebral ischemia during cardiac bypass injury (Nussmeier, 2002), carotid endarterectomy (Jamieson et al., 2003), and resection of aneurysms (Wagner and Zuccarello, 2005) and it is also commonly employed in massive stroke and traumatic brain injury patients (Marion et al., 1996, 1997). Even mild reductions in brain temperature as small as 1°C and importantly, the avoidance of any hyperthermia, can substantially reduce ischemic cell damage (Clark et al., 1996; Wass et al., 1995) and improve outcome (Reith et al., 1996). It seems that either the Pennes or Weinbaum-Jiji bioheat equation alone is unable to predict how the body/blood temperature changes during those situations.

Understanding the blood temperature variation requires a theoretical model to evaluate the overall blood-tissue thermal interaction in the whole body. The theoretical models developed by Wissler and other investigators (Fu, 1995; Salloum, 2005; Smith 1991; Wissler, 1985) similarly introduced the whole body as a combination of multiple compartments. The majority of the previously published studies introduced a pair of countercurrent artery and vein with their respective branching (flow system) in each compartment and then modeled the temperature variations along this flow system to derive the heat transfer between the blood vessels and tissue within each flow segment. The accuracy of those approaches of applying a countercurrent vessel pair and their subsequent branches has not been verified by experimental data. Such an approach is also computationally intensive although the models are capable of delineating the temperature decay along the artery and the rewarming by the countercurrent vein.

A developed whole body model by our group (Zhu et al., 2009a) utilizes the simple representation of the Pennes perfusion source term to assess the overall thermal interaction between the tissue and blood in the human body. As shown in Fig. 4.5, a typical human body (male) has a body weight of 81 kg and a volume of 0.074 m^3. The body consists of limbs, torso (internal organs and muscle), neck, and head. The limbs and neck are modeled as cylinders consisting of muscle. Note that the body geometry can be modeled more realistically if one includes a skin layer and a fat layer in each compartment. However, since our objective is to illustrate the principle and feasibility of the developed model, those details are neglected in the sample calculation. The simple geometry results in a body surface area of 1.8 m^2. Applying the Pennes bioheat equation to the whole body yields

$$\rho_t c_t \frac{\partial T_t}{\partial t} = k_t \nabla^2 T_t + q_m''' + \rho_b c_b \omega (T_a - T_t) \tag{4.10}$$

where subscripts t and b refer to tissue and blood, respectively, T_t and T_a are body tissue temperature and blood temperature, respectively, ρ is density, c is specific heat, k_t is thermal conductivity of tissue, q_m''' is the volumetric heat generation rate (W/m^3) due to metabolism, and ω is the local blood

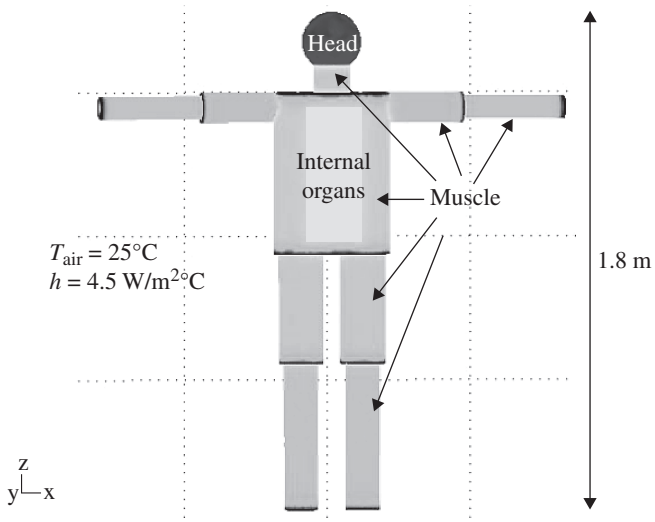

FIGURE 4.5 Schematic diagram of the whole body geometry.

perfusion rate. The above governing equation can be solved once the boundary conditions and initial condition are prescribed. The boundary at the skin surface is modeled as a convection boundary subject to an environment temperature of T_{air} and a convection coefficient of h.

Based on the Pennes bioheat equation, the rate of the total heat loss from the blood to tissue at any time instant is

$$Q_{\text{blood-tissue}} = \iiint_{\text{body volume}} \rho_b c_b \omega (T_a(t) - T_t) dV_{\text{body}} = \rho_b c_b \bar{\omega} (T_a(t) - \bar{T}_t) V_{\text{body}} \tag{4.11}$$

where V_{body} is the body volume, T_a is the blood temperature which may vary with time. Equation (4.11) assumes that both density ρ_b and specific heat c_b of blood are constant. In Eq. (4.11), $\bar{\omega}$ is the average blood perfusion rate defined as

$$\bar{\omega} = \frac{1}{V_{\text{body}}} \iiint_{\text{body volume}} \omega \, dV_{\text{body}} \tag{4.12}$$

In Eq. (4.11), $\bar{T}_t$ is the blood perfusion weighted-average tissue temperature and is defined as

$$\bar{T}_t = \frac{\iiint_{\text{body volume}} \rho_b c_b \omega T_t dV_{\text{body}}}{\rho_b c_b \bar{\omega} V_{\text{body}}} = \frac{\iiint_{\text{body volume}} \omega T_t dV_{\text{body}}}{\bar{\omega} V_{\text{body}}} \tag{4.13}$$

where T_t can be determined by solving the Pennes bioheat equation.

During clinical applications, external heating or cooling of the blood can be implemented to manipulate the body temperature. In the study of Zhu et al. (2009a), the blood in the human body is represented as a lumped system. It is assumed that a typical value of the blood volume of body, V_b, is approximately 5 L. External heating or cooling approaches can be implemented via an intravascular catheter or intravenous fluid infusion. A mathematical expression of the energy absorbed or removed per unit time is determined by the temperature change of the blood, and is written as

$$\rho_b c_b V_b \left[T_a(t + \Delta t) - T_a(t)\right] / \Delta t \approx \rho_b c_b V_b \frac{dT_a}{dt} \tag{4.14}$$

where $T_a(t)$ is the blood temperature at time, t, and $T_a(t + \Delta t)$ is at time $t + \Delta t$. In the mathematical model, we propose that energy change in blood is due to the energy added or removed by external heating or cooling (Q_{ext}), and heat loss to the body tissue in the systemic circulation ($Q_{\text{blood-tissue}}$). Therefore, the governing equation for the blood temperature can be written as

$$\rho_b c_b V_b \frac{dT_a}{dt} = Q_{\text{ext}}(T_a, t) - Q_{\text{blood-tissue}}(t) = Q_{\text{ext}}(T_a, t) - \rho_b c_b \overline{\omega} V_{\text{body}}(T_a - \overline{T}_t) \qquad (4.15)$$

where Q_{ext} can be a function of time and the blood temperature due to thermal interaction between blood and the external cooling approach, T_a, $\overline{T}_t$, and $\overline{\omega}$ can be functions of time. Equation (4.15) cannot be solved alone since $\overline{T}_t$ is determined by solving the Pennes bioheat equation. One needs to solve the coupled Eqs. (4.10) and (4.15) simultaneously.

The developed model in Zhu et al. (2009a) using the Pennes perfusion term and lumped system of the blood is simple to use in comparison with these previous whole body models while providing meaningful and accurate theoretical estimates. It also requires less computational resources and time. Although the model was developed for applications involving blood cooling or rewarming, the detailed geometry can also be used to accurately predict the body temperature changes during exercise. It is well known that strenuous exercise increases cardiac output, redistributes blood flow from internal organs to muscle, increases metabolism in exercising muscle, and enhances heat transfer to the skin. The whole body model can be easily modified to also include a skin layer and a fat layer in the compartments of the limbs. Further, redistribution of blood flow from the internal organs to the musculature can be modeled as changes of the local blood perfusion rate in the respective compartments and the enhanced skin heat transfer can be adjusted for by inducing evaporation at the skin surface and/or taking off clothes to increase the overall heat transfer coefficient (h). Therefore, one can use the model to accurately delineate important clinical scenarios such as heat stroke, and predict body temperature elevations during heavy exercise and/or heat exposures.

One application of blood cooling involves pumping coolant into the inner tube of a catheter inserted into the femoral vein and advanced to the veno-vera. Once the coolant reaches the catheter, it flows back from the outer layer of the catheter and out of the cooling device. This cooling device has been used in clinical trials in recent years as an effective approach to decrease the temperature of the body for stroke or head injury patients. Based on previous research of this device, the cooling capacity of the device is around –100 W [Q_{ext} in Eq. (4.15)].

Figure 4.6 gives the maximum tissue temperature, the minimum tissue temperature at the skin surface, the volumetric-average body temperature (T_{avg}), and the blood perfusion weighted-average body temperature ($\overline{T}_t$). The difference between the volumetric-average body temperature and the blood perfusion weighted-average body temperature is due to their different definitions. All tissue temperatures decrease almost linearly with time and after 20 minutes, the cooling results in approximately 0.3 to 0.5°C tissue temperature drop. The cooling rate of the skin temperature is smaller (0.2°C/20 min). As shown in Fig. 4.7, the initial cooling rate of the blood temperature in the detailed model is very high (~0.14°C/min), and then it decreases gradually until it is stabilized after approximately 20 minutes. On the other hand, cooling the entire body (the volumetric average body temperature) starts slowly and gradually catches up. It may be due to the inertia of the body mass in responding to the cooling of the blood. Figure 4.7 also illustrates that after the initial cooling rate variation, the stabilized cooling rates of all temperatures approach each other and they are approximately 0.019°C/min or 1.15°C/h. The simulated results demonstrate the feasibility of inducing mild body hypothermia (34°C) within 3 hours using the cooling approach.

This whole body model has been used in predicting temperature elevations in a human body when it is subjected to either heavy exercise or immersed into cold water (Paul et al., 2015). Assessment of heat stroke risks in fire fighters has also been evaluated using this model (Devarakonda et al., 2018; Kalathil et al., 2016). Interestingly, the steady-state temperature field of a human body can be predicted using the whole body model, based on the determination of the overall heat transfer coefficient between the skin surface of the body and the ambient environment (Bartgis et al., 2016;

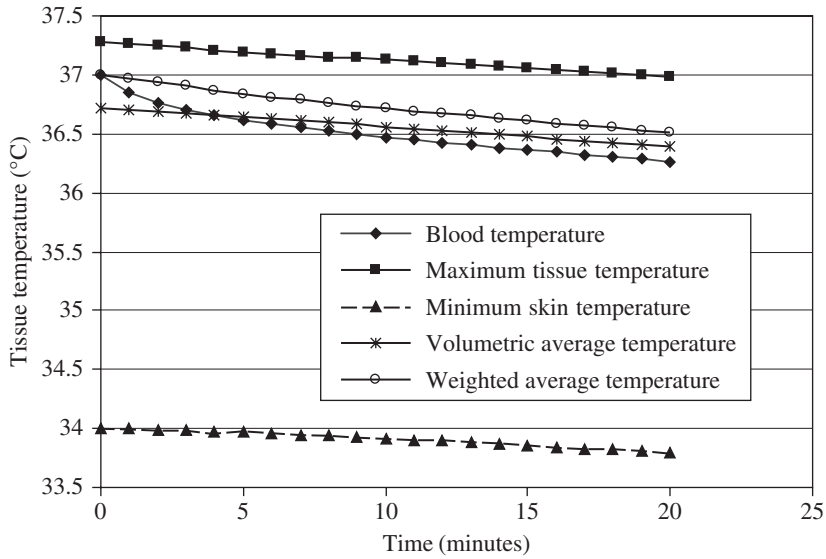

FIGURE 4.6 Temperature decays during the cooling process using the implicit scheme.

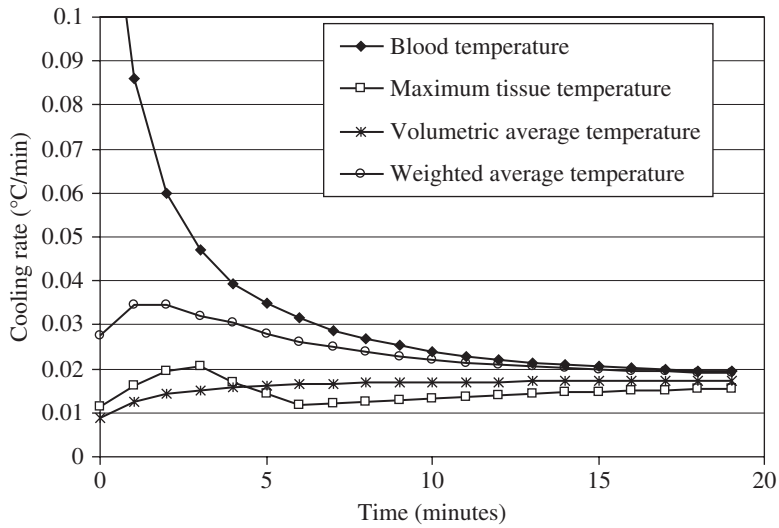

FIGURE 4.7 Induced cooling rates of the blood temperature, the maximum temperature, the volumetric average temperature, and the weighted average temperature.

Vesnovsky et al., 2017). The thermal resistances of clothing layers and convection/radiation are often difficult to evaluate. The whole body model is used to determine the overall heat transfer coefficient during steady state, based on the assumption that a person would dress properly when subject to an ambient environment, to maintain a thermal equilibrium with its environment (Bartgis et al., 2016; Vesnovsky et al., 2017).

4.4 TEMPERATURE, THERMAL PROPERTY, AND BLOOD FLOW MEASUREMENTS

4.4.1 Temperature

The control of human body temperature is a complex mechanism involving release of neurotransmitters and hormones, redistributing blood flow to the skin, respiration, evaporation, and adjusting metabolic rate. The control mechanism can be altered by certain pathologic (fever) and external (hyperthermia treatment) events. Consequently, temperature is an important parameter in the diagnosis and treatment for many diseases. Elevated local tissue temperature can be an indication of excess or abnormal metabolic rates. Inflammation is the body's response to attacks and a mechanism for removing foreign or diseased substances. Exercise also induces an increase in local temperature of skeletal muscles and joints. Some diagnostic procedures involve the measurement of temperatures. Thermal images of the breast surface have been used to detect the presence of malignant tumors. Temperature measurement is also critical in many therapeutic procedures involved in either hyperthermia or hypothermia.

Temperature-measuring devices can fall into two categories, invasive and noninvasive. Invasive temperature sensors offer the advantages of small size, fast response time, extreme sensitivity to temperature changes, and high stability. However, they have generally involved a limited number of measurement locations, uncertainties about the anatomic placement of thermometry devices, interaction with the energy field applied, periodic rather than continuous temperature monitoring, and, in some cases, surgical exposure of the target tissue for placement of the temperature probes.

Invasive temperature devices include thermocouples, thermistor beads, optical fiber sensors, etc. A thermocouple consists of two pieces of dissimilar metal that form two junctions. In the wire, an electric potential difference is formed if there exists a temperature difference between the two junctions. This potential difference can be measured with a high resolution voltmeter and translated to temperature with a fairly simple means of calibration. A thermocouple usually has a good long-term stability, responds very quickly to changes in temperature due to its small thermal capacity, and can be constructed in a manner that allows a good resolution. Another kind of invasive device, the thermistor bead, is made by depositing a small quantity of semiconductor paste onto closely spaced metal wires. The wire and beads are sintered at a high temperature when the material forms a tight bond. The wires are then coated with glass or epoxy for protection and stabilization. The resistors generally exhibit high thermal sensitivity. This characteristic sensitivity to temperature change can result in a change of thermistor resistance of more than 50 $\Omega/^{\circ}$C. Unlike a thermocouple or a thermistor bead, the fiber optic temperature probe does not interfere with an electromagnetic field. It has been used to measure tissue temperature rise induced by microwave and/or radio frequency (RF) heating (Zhu et al., 1996b, 1998). However, it is relatively big in size ($\sim$1.5 mm in diameter) and has a lower temperature resolution ($\sim$0.2°C).

Noninvasive temperature-measuring techniques include MRI thermometry, infrared thermography, etc. Because of the theoretical sensitivity of some of its parameters to temperature, MRI has been considered to be a potential noninvasive method of mapping temperature changes during therapies using various forms of hyperthermia. MRI imaging has the advantage of producing three-dimensional anatomic images of any part of the body in any orientation. In clinical practice, MRI characteristic parameters such as the molecular diffusion coefficient of water, the proton spin-lattice (T_1) relaxation time (Parker et al., 1982), and the temperature-dependent proton resonance frequency (PRF) shift have been used to estimate the in vivo temperature distribution in tissues. MRI provides good spatial localization and sufficient temperature sensitivity. At the present time, it also appears to be the most promising modality to conduct basic assessments of heating systems and techniques. The disadvantages of MRI thermometry include limited temporal resolution (i.e., quasireal time), high environmental sensitivity, high material expenditure, and high running costs.

Infrared thermography is based on Planck's distribution law describing the relationship between the emissive power and the temperature of a blackbody surface. The total radiative energy emitted by an object can be found by integrating the Planck equation for all wavelengths. This integration gives the Stefan-Boltzmann law $E(T) = \varepsilon\sigma T^4$. The thermal spectrum as observed by an infrared-sensitive

detector can be formed primarily by the emitted light. Hence, the formed thermal image is determined by the local surface temperature and the emissivity of the surface. If the emissivity of the object is known, and no intervening attenuating medium exists, the surface temperature can be quantified.

The major challenge of implementing the approach in biological systems is the unknown emissivity values of skin. It has been shown that normal skin emissivity varies from 0.95 to 0.99, depending on skin tone. When the skin is not a perfect blackbody surface, emission from the surrounding may be incident on the skin and portion of it is reflected. Therefore, the irradiation received by the infrared camera consists of contributions of radiation not only from the skin, but also from the surrounding. Many infrared cameras on the market use the following equation to predict temperature, modified from Bernard et al. (2013):

$$T = \sqrt[4]{\frac{q_{ck}}{\sigma\varepsilon} - \frac{1-\varepsilon}{\varepsilon} T_{amb}^{\boxed{4}}} \tag{4.16}$$

where q_{ck} is the heat flux received by the camera and ε is the emissivity of the skin surface. The ambient temperature T_{amb} affects the reading only when the surface is not a blackbody surface. Figure 4.8 gives the deviation of the temperature reading from that when ε is selected as 1, based on inputs of ε and T_{amb} to the recorded infrared image of human skin using a commercial infrared camera. In a room temperature environment ($T_{amb} = 22.5°C$), changing ε from 1 to 0.96 results in an uncertainty of 0.5°C. The potential error is more profound when $T_{amb} = 8.6°C$, with a deviation of 0.83°C (Li et al., 2016). The results from the camera reading are consistent with those predicted by Eq. (4.16).

A numerical simulation of the temperature field of breast (Hu et al., 2004) suggests that image subtraction could be employed to improve the thermal signature of the tumor on the skin surface. Drug-induced vascular constriction in the breast can further enhance the ability of infrared thermography in detecting deep-seated tumor. Qualitative thermography has been successfully used in a wide range of medical applications (Jones, 1998) including cardiovascular surgery (Firorini et al., 1983), breast cancer diagnoses (Gautherie and Gros, 1980; Lapayowker and Revesz, 1980), tumor hyperthermia (Cetas et al., 1980), laser angioplasty, and peripheral venous disease. Clinical studies on patients who had breast thermography demonstrated that an abnormal thermography was associated with an increased risk of breast cancer and a poorer prognosis for the breast cancer

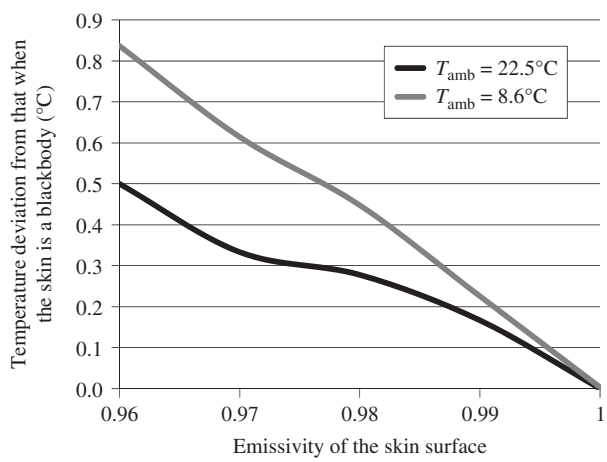

FIGURE 4.8 Effect of skin emissivity and ambient temperature on the temperature reading of a skin location given by the Fluke camera using Eq. (4.16).

patients (Gautherie and Gros, 1980; Head et al., 1993). Infrared tympanic thermometry and temporal thermometry have also been developed and widely used in clinical practice and thermoregulatory research as a simple and rapid device to estimate the body core temperature (Matsukawa et al., 1996; Shibasaki et al., 1998). However, due to uncertainty of the emissivity of tissue surface, large errors may be introduced from the value given by those commercial infrared thermometers, and leading to overestimation or underestimation of actual skin temperature (Li et al., 2016; Vesnovsky et al., 2017).

4.4.2 Thermal Property (Thermal Conductivity and Thermal Diffusivity) Measurements

Knowledge of thermal properties of biological tissues is fundamental to understanding heat transfer processes in biological systems. This knowledge has increased importance in view of the concerns for radiological safety with microwave and ultrasound irradiation, and with the renewed interest in local and regional hyperthermia as a cancer therapy. The availability of a technique capable of accurately characterizing thermal properties of both diseased and normal tissue would greatly improve the predictive ability of theoretical modeling and lead to better diagnostic and therapeutic tools.

The primary requirement in designing an apparatus to measure thermal conductivity and diffusivity is that the total energy supplied should be used to establish the observed nonuniform temperature distribution within the specimen. For accurate measurements, it is important to ensure agreement between the experimental setup and the boundary/initial conditions implemented in the theoretical model. Other structural and environmental factors, such as undesired heat conduction to or from the specimen, convection currents caused by temperature-induced density variations, and thermal radiation, must be minimized if they are not considered in the theoretical model. Biomaterials present additional difficulties. The existing literature on biological heat transfer bears convincing evidence of the complexity of heat transfer processes in living tissue. For example, thermal properties of living tissue differ from those of excised tissue. Clearly the presence of blood perfusion is a major factor in this difference. Relatively large differences in thermal conductivity exist between similar tissues and organs, and variations for the same organ are frequently reported. Such variations suggest the importance of both defining the measurement conditions and establishing a reliable measurement technique.

The thermal property measurement techniques can be categorized as steady-state methods and transient methods. They can also be categorized as invasive and noninvasive techniques. In general, determining thermal properties of tissue is conducted by an inverse heat transfer analysis during which either the temperatures or heat transfer rates are measured in a well-designed experimental setup. The major challenge is to design the experiment so that a theoretical analysis of the temperature field of the experimental specimen can be as simple as possible to determine the thermal property from the measured temperatures. It is usually preferred that an analytical solution of the temperature field can be derived. In the following sections, those principles are illustrated by several widely used techniques for measuring tissue thermal conductivity or diffusivity. Their advantages and limitations will also be described.

Guarded Hot Plate. Thermal conductivity can be measured directly by using steady-state methods, such as the guarded hot plate. This method is invasive in that it requires the excision of the specimen for in vitro measurement. It typically involves imposing a constant heat flux through a specimen and measuring the temperature profile at specific points in the specimen after a steady-state temperature field has been established. Once a simple 1D steady-state temperature field is established in the specimen, the thermal conductivity may be easily found by the expression based on the linear temperature profile in a 1D wall

$$k = \frac{q'' L}{T_1 - T_2} \tag{4.17}$$

where q'' is the heat flux passing through the specimen, T_1 and T_2 are temperature values at any two measurement locations in the axial direction (or the direction of the heat flux), and L is the axial distance between these two temperature measurements.

Biological materials typically have moderate thermal conductivities and therefore, require extensive insulation to ensure a unidirectional heat flow in the 1D wall. The contact resistance between the specimen and the plate is also difficult to be minimized. In addition, this method cannot be used to obtain in vivo measurements. Once the tissue specimen is cut from the body, dehydration and temperature-dependent properties may need to be considered. It is also a challenge to accurately measure the thickness of the tissue sample.

Flash Method. The transient flash method, first proposed by Parker et al. (1961), is the current standard for measuring the thermal diffusivity of solids. A schematic diagram of this method is shown in Fig. 4.9. The front face of a thin opaque solid, of uniform thickness, is exposed to a burst of intense radiant energy by either a high-energy flash tube or laser. The method assumes that the burst of energy is absorbed instantaneously by a very thin layer at the surface of the specimen. Adiabatic boundary conditions are assumed on all other surfaces and on the front face during the measurement. The transient temperature at the rear surface is then measured by using a thermocouple or an infrared detector.

The governing equation can be described by the 1D transient heat conduction problem as

$$\begin{aligned} &\frac{1}{\alpha}\frac{\partial\Theta}{\partial t} = \frac{\partial^2\Theta}{\partial x^2} \\ &x = 0, \quad \text{and} \quad x = l \quad \frac{\partial\Theta}{\partial x} = 0 \\ &t = 0 \quad \begin{cases} \Theta(x,\,0) = \dfrac{Q''A}{\rho c(gA)} & for \quad 0 < x \le g \\ \Theta(x,\,0) = 0 & for \quad g < x \le l \end{cases} \end{aligned}, \tag{4.18}$$

where $\Theta(x,\,t)$ is the temperature elevation and equal to $T(x,\,t) - T(l,\,0)$, Q is the absorbed radiant energy per unit area, g is the thickness of the specimen layer that absorbs all the incident radiant energy, l is the sample thickness, ρ is the density of the specimen, c is the specific heat, and α is the thermal diffusivity of the specimen. Solving the governing equation using the method of separation of variables yields

$$\Theta(x,\,t) = \frac{1}{l}\int_0^l \Theta(x,\,0)dx + \frac{2}{l}\left\{\sum_{n=1}^{\infty}\exp\left(-\frac{n^2\pi^2\alpha t}{l^2}\right)\cos\left(\frac{n\pi x}{l}\right)\left[\int_0^t \Theta(x,\,0)\cos\left(\frac{n\pi x}{l}\right)dx\right]\right\} \tag{4.19}$$

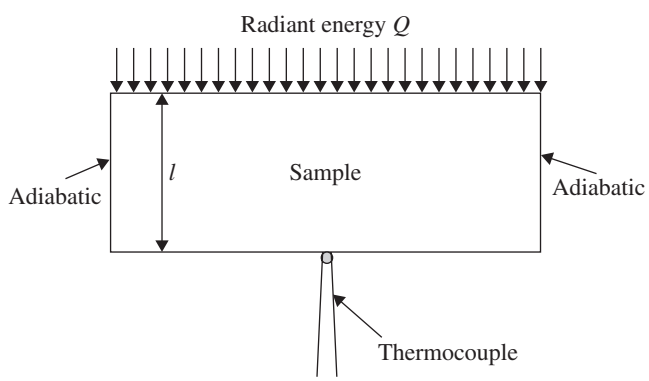

FIGURE 4.9 Schematic diagram of a flash apparatus for sample diffusivity measurements.

The integration in the expression can be derived using the initial condition. After implementing the condition of a very thin layer for energy absorption, i.e., $g \to 0$, one obtains the solution as

$$\begin{aligned} \Theta(x,\ t) &\approx \frac{Q''}{pcl}\left\{1 + 2\sum_{n=1}^{\infty}\exp\left(-\frac{n^2\pi^2\alpha t}{l^2}\right)\cos\left(\frac{n\pi x}{l}\right)\right\} \\ \frac{T(x,\ t) - T(l,\ 0)}{Q''/(\rho cl)} &\approx \left\{1 + 2\sum_{n=1}^{\infty}\exp\left(-\frac{n^2\pi^2\alpha t}{l^2}\right)\cos\left(\frac{n\pi x}{l}\right)\right\} \end{aligned} \tag{4.20}$$

An analytic expression for the rear surface temperature transient in the 1D temperature field is given by

$$\frac{T(l,\ t) - T(l,\ 0)}{Q''/(\rho cl)} \approx \left\{1 + 2\sum_{n=1}^{\infty}\exp\left(-\frac{n^2\pi^2\alpha t}{l^2}\right)\cos(n\pi)\right\} \tag{4.21}$$

In theory, the thermal diffusivity α can be calculated from any set of the recorded temperature and time, i.e., $T(l,\ t_1)$ and t_1. One only needs to substitute the set to Eq. (4.21), and find the root (α) of the equation. Another way to determine the value of the thermal diffusivity of the specimen is to use curve fitting technique to adjust the value of α, until the theoretically predicted temperature transient curve $T(l,\ t)$ has the best fit to the scattered experimental measurements. In industry, the thermal diffusivity in the direction of heat flow is usually calculated by the expression

$$\alpha = 1.38\frac{l^2}{\pi^2 t_{1/2}} \tag{4.22}$$

where $t_{1/2}$ is the time required for the rear surface to reach half of its maximum temperature elevation, the value 1.38 is derived from Eq. (4.21), and it is the most convenient method to quickly determine α.

The simplicity of the method described above is often offset by the difficulty in satisfying the required adiabatic boundary conditions on both top and bottom surfaces. In order for this 1D heat transfer solution to be valid, the radiant energy incident on the front surfaces is required to be uniform, and the duration of the flash must be sufficiently short compared with the thermal characteristic time of the sample. 1D heat conduction in the x direction also implies uniform thickness of the specimen, which adds challenge to biological specimen. The specimen also has to be considered opaque; thus, all the radiant energy is absorbed within a very thin layer. In addition, it assumes that the sample is homogeneous, isotropic, and opaque, and that the thermal properties of the sample do not vary considerably with temperature.

Needle Probe Method. Needle probe method was developed in the 1990s (Liang et al., 1991), and it is based on a derived analytic solution of the temperature field in tissue/specimen surrounding a long needle probe. The needle probe is hollow to host a wire heater inside to mimic an infinite long line source and a thermocouple to measure transient temperature elevations on the needle surface, shown in Fig. 4.10. It requires that the needle can penetrated into the specimen, preferably soft material/tissue. Since the wire heater inside the needle generates heating at a constant level, its dissipation through the specimen relies on the thermal properties of the specimen, thus affecting the rate of temperature elevation rate measured by the temperature sensor at the needle surface.

The theoretical simulation again assumes 1D transient temperature field surrounding a finite long line source in an infinitely large domain. The governing equation for the temperature field $T(r,\ t)$ in the cylindrical coordinate system is written as

$$\begin{aligned} &\frac{1}{\alpha}\frac{\partial T}{\partial t} = \frac{1}{r}\frac{\partial}{\partial r}\left(r\frac{\partial T}{\partial r}\right) + 0 \\ &r = 0 \quad -2\pi rk\frac{\partial T}{\partial r} = q' \\ &t = 0 \quad T = T_i \end{aligned} \tag{4.23}$$

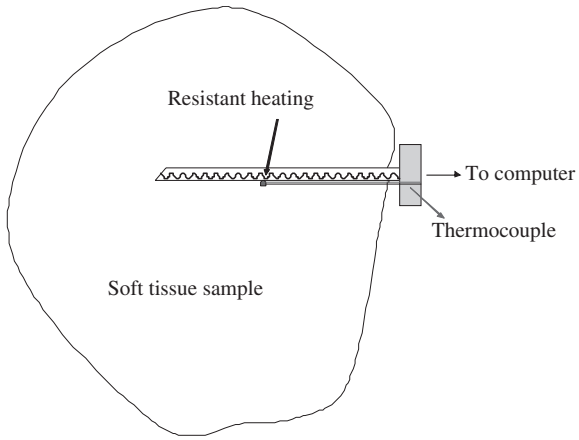

FIGURE 4.10 Schematic diagram of the needle probe for measuring thermal conductivity of a tissue sample.

where q' is the heat transfer rate from the needle probe per unit length of the needle probe, carrying a unit of W/m. The solution for this 1D transient heat conduction problem is given as

$$T - T_i = -\frac{q'}{4\pi k} E_i\left(-\frac{r^2}{4\alpha t}\right) \tag{4.24}$$

where $E_i(-\eta)$ is an exponential integral function defined by

$$E_i(-\eta) = -\int_{\eta}^{\infty} \frac{e^u}{u} du = 0.5772 + \ln \eta + \sum_{n=0}^{\infty} \frac{(-\eta)^n}{n(n!)} \tag{4.25}$$

when η or $r^2/4\alpha t < 0.0256$, the summation portion of Eq. (4.25) can be neglected. The temperature field is then approximated as

$$T - T_i \approx \frac{q'}{4\pi k}\left[\ln\left(\frac{4\alpha t}{r^2}\right) + 0.5772\right] = \frac{q'}{4\pi k}\ln t + \frac{q'}{4\pi k}\left[\ln\left(\frac{4\alpha}{r^2}\right) + 0.5772\right] \tag{4.26}$$

At the needle surface when $r = r_0$, the transient temperature elevation is given as

$$T(r_0, t) - T_i \approx \frac{q'}{4\pi k}\ln t + \frac{q'}{4\pi k}\left[\ln\left(\frac{4\alpha}{r_0^2}\right) + 0.5772\right] \tag{4.27}$$

After plotting the measured temperature above its initial value as a function of $\ln t$, the curve should be linear with a slope equal to $q'/(4\pi k)$. The thermal conductivity can be obtained from the above equation as

$$k = \frac{q'}{4\pi}\frac{d(\ln t)}{dT(r_0, t)} \tag{4.28}$$

This relationship suggests that the faster the temperatures rises, the material is more likely to be poorly conductive. On the other hand, if the material is highly conductive, heat from the needle can be dissipated easily, therefore, resulting in a slower temperature rise at the needle surface. Once the thermal conductivity k is obtained, the thermal diffusivity of the specimen can be calculated based

on the temperature measurement $T(r_0, t_c)$ at any time instance t_c, at the location $r = r_0$. Rearranging Eq. (4.27), one obtains the following equation to calculate the thermal diffusivity of the specimen:

$$\alpha = \frac{r_0^2}{4t_c}\exp\left\{\frac{4\pi k}{q'}[T(r_0, t_c) - T_i] - 0.5772\right\} \tag{4.29}$$

Errors of this method are largely due to deviation of the experimental setup, including geometry and boundary conditions from the idealized 1D heat transfer with a line source in an infinite domain. The needle probe should be sufficiently long to satisfy the line source requirement. The specimen should be penetrated to minimize air gap between the needle probe surface and material of the specimen. Depending on the thermal diffusivity of the material, it may take a long time to reach the linear portion of the temperature rising curve, i.e.,

$$t_1 \geq \frac{r_0^2}{4\alpha * 0.0256} \tag{4.30}$$

Another potential error is due to difficulty to satisfy the infinite domain requirement. When heat is transferred from the needle probe to the edge of the specimen, the boundary condition at the specimen surface would violate the requirement of the infinite domain. Therefore, the linear relationship given in Eq. (4.28) would not be valid after a specific time t_2, given by

$$t_2 = \frac{L^2}{4\alpha} \tag{4.31}$$

where L is the minimum distance from the sample boundary to the probe axis. Due to the small thermal diffusivity of biological tissue, it may take some time to reach t_1; however, it may also take a much longer time for the heat to reach the specimen boundary, thus allowing sufficient measurement points for linear curve fitting. Iterations may also be needed due to unknown thermal diffusivity before the measurements. One often has to guess its value to evaluate both t_1 and t_2, and later to readjust the value of α to ensure that only the measurement points in the linear portion of the curve are used for curve fitting.

Temperature Pulse Decay (TPD) Technique. Temperature pulse decay (TPD) technique is based on the approach described and developed by Arkin, Chen, and Holmes (Arkin et al., 1986, 1987). This method needs no insulation, in contrast to some of the methods described above, since testing times are short, usually on the order of seconds. However, the determination of the thermal conductivity or the blood flow rate requires the solution of the transient bioheat transfer equation.

This technique employs a single thermistor serving as both a temperature sensor and a heater. Typically in this technique, either a thermistor is inserted through the lumen of a hypodermic needle, which is in turn inserted into the tissue, or the thermistor is embedded in a glass-fiber-reinforced epoxy shaft. Figure 4.11 shows the structure of a thermistor bead probe embedded in an epoxy shaft and its insertion into tissue. Each thermistor bead probe can consist of one or two small thermistor beads situated at the end or near the middle of the epoxy shaft. The diameter of the finished probe is typically 0.3 mm, and the length can vary as desired. Because the end can be sharpened to a point, it is capable of piercing most tissues with very minimal trauma.

During the experiment, the thermistor bead probe is inserted into the tissue of interest. A short heating pulse of approximately 3 seconds is delivered by the thermistor bead. The pulse heating results in a temperature rise in the area near the tip of the probe. After the pulse heating, the temperature of the probe will decrease. During the pulse heating and its subsequent temperature decay, the temperature at the tip of the probe is measured by the thermistor bead. To determine the thermal conductivity or blood flow rate, a theoretical prediction of the transient temperature profile is needed for the same tissue domain as in the experimental study. Typically, the theoretically predicted temperature profile is obtained by solving a bioheat transfer equation in which the blood flow rate and thermal conductivity have to be given as input to the model. The predicted temperature profile is then compared with the experimental measurements. The values of the blood flow rate and/or thermal conductivity will be adjusted to minimize the square difference between the predicted temperature

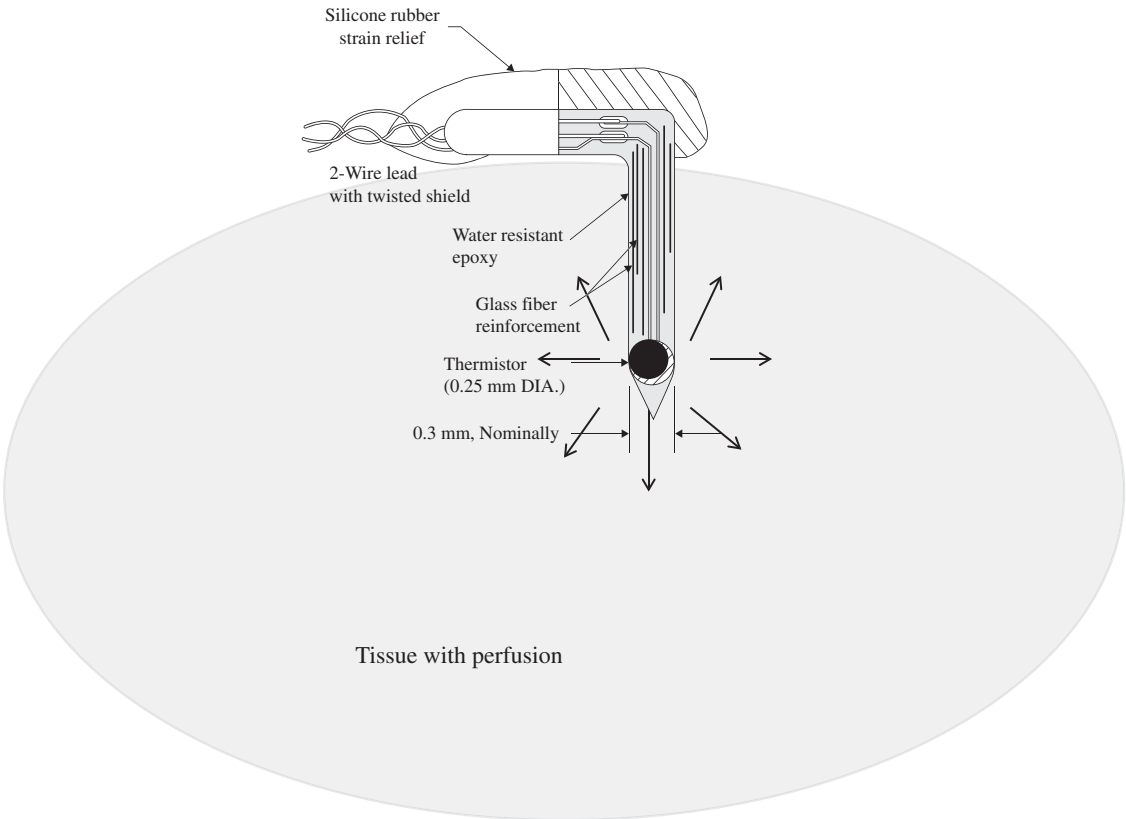

FIGURE 4.11 Sketch of a thermistor bead probe inserted into a tissue region. [*From Xu et al. (1998) with permission.*]

profile and the experimental measurements using the linear-square residual fit. The values for the blood flow rate and thermal conductivity that give the best fit of the experimentally measured temperature profile are the calculated blood flow rate and thermal conductivity of the tissue sample.

Typically, the Pennes bioheat transfer equation is used to predict the temperature transient. It is assumed that the thermistor bead is small enough to be considered a point source inserted into the center of an infinitively large medium. The governing equation and initial condition for this thermal process are described as

$$\begin{aligned} &\rho_t c_t \frac{\partial T_t}{\partial t} = k_t \frac{1}{r}\frac{\partial}{\partial r}\left(r\frac{\partial T_t}{\partial r}\right) + \omega\rho_b c_b (T_a - T_t) + q_p \\ &t = 0, \qquad T_t = T_{ss}(r) \end{aligned} \tag{4.32}$$

where q_p is the pulse heating deposited locally into the tissue through a very small thermistor bead probe as $q_p = P\ \delta(0)$ for $t \le t_p$; $q_p = 0$ for $t > t_p$. P is the deposited power, and $\delta(0)$ is the Dirac delta function. Before the measurement, the steady-state temperature distribution $T_{ss}(r)$ in the sample should satisfy the 1D steady-state conduction equation without the pulse heating. The governing equation for $T_{ss}(r)$ is given by

$$0 = k_t \frac{1}{r}\frac{d}{dr}\left(r\frac{dT_{ss}}{dr}\right) + \omega\rho_b c_b (T_a - T_{ss}) \tag{4.33}$$

Subtracting Eq. (4.33) from Eq. (4.32), and introducing $\theta = T_t - T_{ss}$, one obtains

$$\rho_t c_t \frac{\partial \theta}{\partial t} = k_t \frac{1}{r}\frac{\partial}{\partial r}\left(r\frac{\partial \theta}{\partial r}\right) + \omega \rho_b c_b \theta + q_p \qquad (4.34)$$
$$t = 0, \qquad \theta = 0$$

For the limiting case of an infinitesimally small probe with an infinitesimally short heating pulse, the solution for Eq. (4.20) for the interval of temperature decay takes the form

$$\theta = \lambda_2 \int_0^{t_0} (t-s)^{-1.5} e^{-\omega(t-s)} e^{-r^2/[4\lambda_1(t-s)]}\, ds \qquad (4.35)$$

where $\lambda_1 = P(\rho_t c_t)^{0.5}/(8\pi^{1.5})$ and $\lambda_2 = \alpha_t/(k_t^{1.5} t_p^{0.5})$. In this theoretical analysis, there are two unknowns, k_t and ω. The least-square residual fit allows one to find a set of values of k_t and ω that will lead to the best fit of the theoretical predictions to the experimentally measured temperature decay.

The TPD technique has been used to measure both the in vivo and in vitro thermal conductivity and blood flow rate in various tissues (Xu et al., 1991, 1998). The specimen does not need to be cut from the body, and this method minimizes the trauma by sensing the temperature with a very small thermistor bead. For the in vitro experimental measurement, the measurement of thermal conductivity is simple and relatively accurate. The infinitively large tissue area surrounding the probe implies that the area affected by the pulse heating is very small in comparison with the tissue region. This technique also requires that the temperature distribution before the pulse heating should reach steady state in the surrounding area of the probe.

4.4.3 Blood Perfusion Measurement

Blood perfusion rate is defined as the amount of blood supplied to a certain tissue region per minute per 100 g tissue weight. In most of the situation, it is representing the nutrient need in that tissue area. High blood perfusion is also associated with heat dissipation during exercise or thermal stress. In humans, there are several tissue regions, such as kidney, heart, and choriocapillaris in the eye, possessing a high blood perfusion rate. The measured blood perfusion rate in the kidney is approximately 500 mL/min/100 g tissue (Holmes, 1997). In the heart, the blood perfusion rate is about 300 mL/min/100 g which serves for the energy need of pumping the heart. The choriocapillaris in the eyes is a meshed structure within two thin sheets. Its blood perfusion rate is very high and can be as much as 8000 mL/min/100 g tissue. In addition to providing oxygen and other nutrients to the retina, the choriocapillaris also may play a role in stabilizing the temperature environment of the retina and retinal pigment epithelium (RPE) (Aurer and Carpenter, 1980). In addition to its physiological role, blood perfusion measurement is important in theoretical modeling of the temperature distribution during various therapeutic and diagnostic applications.

Radio-Labeled Microsphere Technique. Measurement of blood flow has become an integral part of the physiologic study of humans. While many methods have been utilized in measuring tissue blood flow, the one most often practiced today is dependent on injection of radioactively labeled microspheres. The reason for its overwhelming acceptance is due, in part, to the shortcomings of many of the alternative methods of blood flow determination.

In principle, small particles are uniformly mixed with blood and allowed to circulate freely until they impact in a vessel smaller in diameter than themselves. The tissue or organ is then removed and its radioactivity measured. In such a system, the number of particles impacted in a given tissue is assumed proportional to the volume of particle-containing blood perfusing that tissue. If the number of particles in the tissue sample is determined, and an adequate blood flow reference established, a tissue blood flow can be derived.

Calculating the blood flow rate is straightforward; it is based on the assumption that the number of microspheres in each organ should be directly proportional to blood flow to that organ, e.g.,

$$\frac{\text{Blood flow to organ A}}{\text{Microspheres in organ A}} = \frac{\text{Blood flow to organ B}}{\text{Microspheres in organ B}} = \frac{\text{Cardiac output}}{\text{Total microspheres injected}} \quad (4.36)$$

The cardiac output of the animal is obtained by another independent method.

Like any other experimental method, determination of blood flow by radioactive microspheres is subject to many sources of error, including individual variation among the sample population, the counting accuracy of the total microspheres in the tissue sample by the gamma counter, and the effect of arteriovenous shunting or the migration of the microspheres. Despite all the limitations of this method, the microsphere technique of blood flow determination has become the most powerful method available today and has been used to evaluate the accuracy of other techniques of blood flow measurement.

Doppler Ultrasound. Doppler ultrasound has been widely used to provide qualitative measurements of the average flow velocity in large- to medium-size vessels if the vessel diameter is known. These include the extracranial circulation and peripheral limb vessels. It is also used in an assessment of mapped occlusive disease of the lower extremities. The frequency used for Doppler ultrasound is typically between 1 and 15 MHz. The basis of this method is the Doppler shift, which is the observed difference in frequency between sound waves that are transmitted from simple piezoelectric transducers and those that are received back when both transmitter and receiver are in relative motion. The average frequency shift of the Doppler spectrum is proportional to the average particulate velocity over the cross-sectional area of the sample. When used to measure blood flow, the transducers are stationary and motion is imparted by the flowing blood cells. In this event, red cell velocity V is described by the relationship

$$\delta F/F = (2V/C)\cos\theta \qquad \text{or} \qquad V = \delta F/F\,(C/2\cos\theta) \quad (4.37)$$

where δF is the frequency change of the emitted wave, C is the mean propagation velocity of ultrasound within tissues (about 1540 m/s), and θ is the angle between the ultrasound beam and the flow velocity. The frequency shift is usually in the audible range and can be detected by an audible pitch variation or can be plotted graphically.

Attenuation of ultrasound increases nearly linearly with frequency in many types of tissue, causing high frequencies to be attenuated more strongly than low frequencies. The depth of penetration of the signal also depends on the density of the fluid; hence sampling of the velocity profile could be inaccurate in situations where this can vary. Determination of absolute flow/tissue mass with this technique has limited potential, since vessel diameter is not accurately measured and volume flow is not recorded. It is not possible, using currently available systems, to accurately measure the angle made by the ultrasonic beam and the velocity vector. Thus, Doppler flow measurements are semiquantitative.

Laser Doppler Flowmetry. Laser Doppler flowmetry (LDF) offers the potential to measure flow in small regional volumes continuously and with repetitive accuracy. It is ideally suited to measure surface flow on skin or mucosa or following surgical exposure. LDF couples the Doppler principle in detecting the frequency shift of laser light imparted by moving red blood vessels in the blood stream. Incident light is carried to the tissue by fiber optic cables, where it is scattered by the moving red blood cells. By sampling all reflected light, the device can calculate flux of red blood cells within the sample volume. Depending on the light frequency, laser light penetrates tissue to a depth of less than approximately 3 mm.

The output from LDF is measured not in easily interpretable units of flow but rather in hertz. It would be ideal to define a single calibration factor that could be used in all tissues to convert laser output to flow in absolute units. Unfortunately, the calibration to determine an absolute flow is limited by the lack of a comparable standard and the lack of preset controlled conditions. This may be due to varying tissue optical properties affected by tissue density (Obeid et al., 1990). Further, LDF signals can be affected by movement of the probe relative to the tissue.

Despite its limitations, LDF continues to find widespread applications in areas of clinical research because of its small probe size, high spatial and temporal resolution, and entire lack of tissue contact if required. It has been suggested that LDF is well suited for comparisons of relative changes in blood flow during different experimental conditions (Smits et al., 1986). It is especially valuable to provide a direct measurement of cutaneous blood flow. In patients with Raynaud's phenomenon, it has been indicated that the abnormal cutaneous blood flow is related to the diminished fibrinolytic activity and increased blood viscosity (Engelhart and Kristensen, 1986). LDF has also been useful for assessing patients with fixed arterial obstructive disease of the lower extremity (Schabauer and Rooke, 1994). Other cutaneous uses of LDF include postoperative monitoring of digit reattachment, free tissue flap, and facial operations (Schabauer and Rooke, 1994). In the noncutaneous application of LDF, it has been reported to measure the retinal blood flow in patients with diabetes mellitus. LDF has also been used to monitor cerebral blood perfusion (Borgos, 1996). It was used to evaluate the brain autoregulation in patients with head injury (Lam et al., 1997).

Temperature Pulse Decay Technique. As described in the section "Temperature Pulse Decay (TPD) Technique," local blood perfusion rate can be derived from the comparison between the theoretically predicted and experimentally measured temperature decay of a thermistor bead probe. The details of the measurement mechanism have been described in that section. The TPD technique has been used to measure the in vivo blood perfusion rates of different physical or physiological conditions in various tissues (Xu et al., 1991, 1998; Zhu et al., 2005). The advantages of this technique are that it is fast and induces little trauma. Using the Pennes bioheat transfer equation, the intrinsic thermal conductivity and blood perfusion rate can be simultaneously measured. In some of the applications, a two-parameter least-square residual fit was first performed to obtain the intrinsic thermal conductivity of the tissue. This calculated value of thermal conductivity was then used to perform a one-parameter curve fit for the TPD measurements to obtain the local blood perfusion rate at the probe location.

The error of blood perfusion measurement using the TPD technique is mainly inherited from the accuracy of the bioheat transfer equation. Theoretical study (Xu et al., 1993) has shown that this measurement is affected by the presence of large blood vessels in the vicinity of the thermistor bead probe. Further, poor curve fitting of the blood perfusion rate occurs if the steady state of the tissue temperature is not established before the heating (Xu et al., 1998). The TPD method can also be used to measure local blood perfusion rate repeatedly, as long as the steady state of the tissue temperature before each pulse heating can be satisfied. In one application (Zhu et al., 2005), a TPD probe has been used to measure real-time blood perfusion rate in prostatic tissue during transurethral RF heating. The results not only confirmed the general trend of increase in blood perfusion rate with rising tissue temperature, but also illustrated the first time that the local blood perfusion increase lagged behind the temperature rise. Simultaneous measurements of temperature and blood perfusion rate at the same tissue location demonstrated coupled relationship between them (Zhu et al., 2005), suggesting that large temperature rise or temperature threshold triggered an increase in local blood perfusion rate, while large blood perfusion rate led to temperature drop. Unfortunately, the local blood perfusion rate would not be measured more frequently than the temperatures in that study, due to time required to establish a steady state before the heating pulse. A typical duration of measuring blood perfusion rate using TPD is more than 1 minute.

4.5 HYPERTHERMIA TREATMENT FOR CANCERS AND TUMORS

4.5.1 Introduction

Within the past three decades, there have been important advances in the use of hyperthermia in a wide variety of therapeutic procedures, especially for cancer treatment. Hyperthermia is used either as a singular therapy or as an adjuvant therapy with radiation and drugs in human malignancy. It has fewer complications and is preferable to more costly and risky surgical treatment

(Dewhirst et al., 1997). The treatment objective of current therapy is to raise tumor temperature higher than 43°C for periods of more than 30 to 60 minutes while keeping temperatures in the surrounding normal tissue below 43°C. It has been suggested that such elevated temperatures may produce a heat-induced cytotoxic response and/or increase the cytotoxic effects of radiation and drugs. Both the direct cell-killing effects of heat and the sensitization of other agents by heat are phenomena strongly dependent on the achieved temperature rise and the heating duration.

One of the problems encountered by physicians is that current hyperthermia technology cannot deliver adequate power to result in effective tumor heating of all sites. The necessity of developing a reliable and accurate predictive ability for planning hyperthermia protocols is obvious. The treatment planning typically requires the determination of the energy absorption distribution in the tumor and normal tissue and the resulting temperature distributions. The heating patterns induced by various hyperthermia apparatus have to be studied to focus the energy on a given region of the body and provide a means for protecting the surrounding normal tissues. Over the past decades, optimization of the thermal dose is possible with known spatial and temporal temperature distribution during the hyperthermia treatment. However, large spatial and temporal variations in temperature are still observed because of the heterogeneity of tissue properties (both normal tissue and tumor), spatial variations in specific absorption rates, and the variations and dynamics of blood flow (Overgaard, 1987). It has been suggested that blood flow in large, thermally unequilibrated vessels is the main cause for temperature nonhomogeneity during hyperthermia treatment, since these large vessels can produce cold tracts in the heated volume. Thus, to heat the tissue and tumor volume effectively and safely, it is critical to experimentally or theoretically monitor the temporal and spatial temperature gradient during the hyperthermia treatment.

4.5.2 Temperature Monitoring during Thermal Treatment

One of the reasons hyperthermia has not yet become widely accepted as a mode of therapy is the lack of noninvasive and inexpensive temperature measurement technology for routine use. Invasive temperature devices have a number of restrictions when applied to temperature monitoring during hyperthermia. These restrictions include small representative tissue sample of the entire tissue and tumor regions, difficulty in inserting the sensor into a deep-seated tumor, and discomfort to patients during the insertion. Because of the problems associated with invasive temperature measurement techniques, there has been a strong demand for noninvasive temperature feedback techniques such as ultrasonic imaging and microwave radiometry imaging (MRI). In addition to their focusing and real-time capabilities, ultrasound-based techniques are capable of providing satisfactory temperature resolution as well as hot-spot localization in soft tissue. MRI was applied as a noninvasive thermometry method, but it has limited temperature resolution (~0.5°C) and spatial resolution (~1 cm) and, therefore, can provide only an estimate of the average temperature over a certain tissue volume. Further, MRI is a costly technique, and therefore, it does not comply with the clinical requirements of treatment monitoring for tissue temperature distribution.

4.5.3 Heating Patten Induced by Hyperthermia Applicators

Ideal Treatment Volume and Temperature Distribution. Heating pattern induced by external devices is defined as the heat energy deposited in the tissue or tumor per second per unit mass [specific absorption rate (SAR)] or per unit volume of tissue (q'''). In optimal treatment planning, it is the temperature rather than the heating pattern that is optimized in the treatment plan. The maximum temperature generally occurs in the tissue region with heat deposition. However, one should note that SAR and temperature distribution may not have the same profile, since temperature distribution can also be affected by the environment or imposed boundary conditions.

The thermal goal of a clinically practical hyperthermia treatment is to maximize the volume of tumor tissue that is raised to the therapeutic temperature. This maximization should be accomplished while keeping the volume of normal tissue at or below some clinically specific temperature level.

There are difficulties to reaching the optimal temperature distribution with the presently available heating devices. Most clinical heating systems have had such fixed power deposition patterns that optimization was limited. In recent years, the cooperation between engineers and clinicians has resulted in a new generation of heating equipment. These heating devices have considerably more flexibility in their ability to deposit power in different patterns that help reach the treatment goal. Further, the ideal temperature distribution may be achieved by manipulating the geometrical consideration or regional blood flow. In most of the transurethral microwave catheters, circulated cold water is installed in the catheter to provide protection to the sensitive prostatic urethra. Manipulation of the flow rate and temperature of the water have been demonstrated to facilitate the achievement of high temperature penetrating deep in the transition zone (Liu et al., 2000). Preheating the large arterial blood to some extent before it enters the treatment region has also been shown to improve the temperature homogeneity in that area.

Currently Used Heating Approaches. It is known that the size and location of the tumor have a significant impact on applicator design and type of heating. Earlier hyperthermia approaches in the 1980s and 1990s included high-energy DC shock (electric conductive heating), RF (alternating current), microwave (electromagnetic wave absorption), ultrasound (sound wave), laser (electromagnetic wave absorption), etc. All the methods require either a wave or a current passing through the tissue and its interaction with molecules in the tissue to generate heating. The wave or current decays as it passes through the tissue, resulting in a heating density diverging from the location where the wave or current is initiated. Collateral thermal damage to healthy tissue may occur if the targeted tissue region is not located very close to the initiation. Actively cooling the healthy tissue region has been shown to be effective to minimize undesired thermal damage. Recent heating methods such as magnetic nanoparticle hyperthermia and laser photothermal therapy are focused on confining heat generation within targeted tumors, thus minimizing collateral thermal damage to healthy tissue. In this section, different heating devices are introduced and their advantages and limitations are described.

In electric cardioversion, high-energy DC shock (Scheinman et al., 1982) has been used as an implanted energy source for the treatment of drug-refractory supraventricular arrhythmias. During the catheter ablation, the peak voltage and current measured at the electrode-tissue interface are typically higher than 1000 V and 40 A, respectively. Although thermal ablation is not an objective of the approach, the high voltage pulse may result in a very high temperature at the electrode surface. Explosive gas formation and a shock wave can occur, which may cause serious complications, including ventricular fibrillation, cardiogenic shock, and cardiac peroration.

Alternating current in the radio frequency range has been investigated as an alternative to shock for heating applicator (Huang et al., 1987; Nath and Haines, 1995; Nath et al., 1994; Wonnell et al., 1992; Zhu and Xu, 1999). Similar to a DC shock, two electrodes or one electrode and a ground pad are needed and local temperature elevations are due to ohmic heating. RF ablation has been successfully used to treat liver neoplasms, solid renal mass, and osteoid osteomas. In recent years, this technique has been applied to destroy brain tissue for the treatment of motor dysfunctions in advanced Parkinson's disease (Kopyov et al., 1997; Linhares and Tasker et al., 2000; Oh et al., 2001; Patel et al., 2003; Su et al., 2002). The current clinical practice of inducing RF lesions in the brain involves implanting a microelectrode-guided electrode and applying RF current to the targeted region, in order to relieve symptoms of the Parkinson's disease in patients whose symptoms cannot be controlled with traditional pharmacological treatment. Clinical evidence suggests that RF ablation has high success rates in patients with colorectal cancer, with only a few unresectable hepatic metastases (<30 mm diameter); in these patients, the 5-year survival rate varies from 14 to 55 percent. A recent study (Zou et al., 2010) using RF for unresectable pancreatic cancer indicated a marked decrease in pain score and improvements in patients. For prostate cancer treatment, local hyperthermia has been considered minimally invasive due to transurethral or transrectal access to the prostate. The effect of RF ablation was examined in another clinical study (Lanuti et al., 2009) for treating inoperable lung cancer and it has shown 78 and 47 percent survival rates after 2 and 4 years, respectively. It has been reported that high-intensity, focused ultrasound has achieved more than 66 to 80 percent success rate in destroying tumors (Chaussy and Thuroff, 2001; Gelet et al., 2001).

RF energy is readily controllable, and the equipment is relatively cheap (Hariharan et al., 2007a). The standard RF generator used in catheter ablation produces an unmodulated sinusoidal wave alternating current at a frequency of 200 to 1000 kHz. Resistive current density is inversely proportional to the square of the distance from the electrode. Thus, resistive heating decreases with the distance from the electrode to the fourth power. Maximal power occurs within a very narrow rim of tissue surrounding the electrodes. The heating typically leads to desiccation of tissue immediately surrounding the catheter electrodes, but diverges and decreases in-between, which can cause broad variations of heating. Improved RF hyperthermia systems have been proposed to reduce the heterogeneity of the RF heating, including implanting a feedback power current system (Astrahan and Norman, 1982; Hartov et al., 1994) and using electrically insulating material around the electrodes (Cosset et al., 1986).

Microwave hyperthermia uses radiative heating produced by high-frequency power. High-frequency electromagnetic waves may be transmitted down an appropriately tuned coaxial cable and then radiated into the surrounding medium by a small antenna. The mechanism of electromagnetic heating from a microwave source is dielectric rather than ohmic. The heating is due to a propagating electromagnetic wave that raises the energy of the dielectric molecules through which the field passes by both conduction and displacement currents. While maintaining alignment with the alternating electric field, neighboring energized dipole molecules collide with each other and the electromagnetic energy is transformed into thermal energy. The main limitation of microwave heating is that the energy is absorbed within a very narrow region around the microwave antenna. Typically, the generated heat decays fast and can be approximated as proportional to $1/r^2$. The highly absorptive nature of the water content of human tissue has limited the penetration of electromagnetic energy to 1 to 2 cm.

Laser photocoagulation is a form of minimally invasive thermotherapy in which laser energy is deposited into a target tissue volume through one or more implanted optical fibers. Laser is used in medicine for incision and explosive ablation of tumors and other tissues, and for blood vessel coagulation in various tissues. Laser light is nearly monochromatic. Most popular lasers utilized in the laboratory include Argon laser (488 nm), pulsed dry laser (585–595 nm), Nd:YAG lasers operating at 1064 nm, and diode lasers operating at 805 nm. Laser-beam power ranges from milliwatts to several watts. Usually the laser energy is focused on a small tissue area of a radius less than 300 μm, resulting in a very high heat flux or volumetric heat generation rate. Because there is minimal penetration of laser energy into the tissue, sufficient energy is delivered to heat tissues surrounding the point of laser contact to beyond 60°C or higher, leading to denaturation and coagulation of biomolecules. Due to the high-temperature elevation in the target tissue, laser photocoagulation may produce vapor, smoke, browning, and char. A char is usually formed when temperature is elevated above 225°C or higher (LeCarpentier et al., 1989; Thomsen, 1991; Torres et al., 1990; Whelan and Wyman, 1999).

In the three primary clinical applications using laser, dermatologists and ophthalmologists are mostly using laser for blood vessel coagulation, and dentists use lasers in both soft and hard tissue ablation. The selection of laser type is largely determined by how deep the targeted region is located in the tissue. Typically, longer wavelength lasers penetrate more deeply into tissue than short wavelength lasers. One example is in laser coagulation of blood vessels in the eyes. Lasers can penetrate the vitreous easily with only minor absorptions (~5 percent) and reach the retina. Conventional treatment for superficial retinal arteries and veins utilizes short wavelength lasers such as Argon laser (527 nm). It will not be suitable for treating deep choroidal feeder vessels (Flower, 2002). Laser energy must penetrate the overlying retinal layer, RPE, and choriocapillaris to reach the targeted choroidal feeder vessels. Previous experimental and theoretical studies have suggested using a near-infrared (NIR) laser such as diode laser at 805 nm wavelength to deliver sufficient laser energy to the choroidal feeder vessels with minimal concomitant retinal and choroidal damage, especially to the sensitive RPE layer (Banerjee et al., 2007; Flower, 2002; Zhu et al., 2008, 2009b).

Similar approaches can be seen in using laser for treatment of port wine stains (PWS), birthmarks due to deep dilated capillaries located superficially in the skin (Jia et al., 2006). The absorption of laser occurs largely due to oxyhemoglobins (HbO_2) and deoxyhemoglobins (Hb) in the blood stream. Short-wavelength lasers, such as pulsed dye laser (PDL) at 577 and 595 nm and potassium titanyl phosphate (KTP) laser at 532 nm strongly absorbed by both oxyhemoglobin and deoxyhemoglobin,

have been shown effective to obliterate the blood vessels to improve the skin tone in PWS located less than 1 mm beneath the skin surface (Huikeshoven et al., 2007; Jasim and Handley, 2007). However, for deeply seated PWS, it has been proposed to use Alexandrite 755-nm laser or Nd:YAG laser at 1064 nm, which can penetrate into several millimeters in skin tissue. In addition, coagulation of venous blood with rich deoxyhemoglobins is preferred to use Alexandrite laser since the absorption by Hb at 755-nm wavelength is stronger than the absorption by HbO_2. On the other hand, the Nd:YAG laser at 1064 nm is better for obliteration of arterioles since it is absorbed more by HbO_2 than by Hb. In recent years, it has been proposed to use a dual laser system (short- and long-wavelength lasers) targeting both superficial and deep blood vessels in a combined approach (Izikson et al., 2009). Thermal damage to the epidermis (~60 μm in thickness) may occur even with limited laser energy absorption there. One approach to minimize the thermal damage in epidermis is to use cryogen sprayed on the skin surface before or during laser treatment. Theoretical simulations have been performed to identify suitable cooling parameters for preventing collateral thermal damage while delivering sufficient laser energy to the targeted blood vessels located in the dermis.

In dentistry, both short-wavelength lasers such as Nd:YAG, argon, and diode lasers and long wavelength Er;YAG and Er,Cr;YSGG are used in cutting hard tissue, reshaping gums and implants, and removing debris. Recently, bacterial disinfection in deep dentin area using Er,Cr;YSGG lasers has been proposed for root canal procedures (Zhu et al., 2009b). In addition, simple red lasers at 695 nm emitted from a small probe have been used for diagnosis of caries hidden inside the teeth (Barberia et al, 2008; Chu et al., 2010). Comparing to dermatology and ophthalmology, there are relatively limited studies in dentistry to optimize treatment efficacy when selecting from a variety of lasers. There are also only a few studies to evaluate collateral thermal damages to the tissue surrounding the targeted tooth region.

Unlike the electromagnetic heating devices mentioned above, ultrasound heating is a mechanical hyperthermic technique. The acoustic energy, when absorbed by tissue, can lead to local temperature rise. Modern ultrasound systems use a curved transducer placed on the skin surface, making this the least invasive in the methods. The focal point due to the curvature of the transducer can be adjusted to focus heating mostly on the region of interest. Ultrasound offers many advantages as an energy source for hyperthermia because of its small wavelength and highly controllable power deposition patterns, including penetration depth control in human soft tissue (Hariharan et al., 2007a, 2007b). The depth of the resulting lesion could theoretically be increased or decreased by selecting a lower or higher ultrasound frequency, respectively. It has been shown that scanned focused ultrasound provides the ability to achieve more uniform temperature elevations inside tumors than the electromagnetic applicators. Moros and Fan (1998) have shown that the frequency of 1 MHz is not adequate for treating chest wall recurrences, since it is too penetrating. As for a deep-seated tumor (3 to 6 cm deep), longer penetration depth is achieved by using relatively low frequency (1 MHz) and/or adjusting the acoustic output power of the transducer (Moros et al., 1996). The practical problem associated with ultrasound heating is the risk of overheating the surrounding bone–tissue interface because of the high ultrasound absorption in bone.

Another hyperthermia approach involves microparticles or nanoparticles which can generate heat in tissue when subjected to an alternating magnetic field. Magnetic particle hyperthermia procedure consists of localizing magnetic particles within tumor tissue or tumor vasculature and applying an external alternating magnetic field to agitate the particles (Gilchrist et al., 1957). In this case, magnetic particles function as a heat source, which generates heat due to hysteresis loss, Néel relaxation, Brownian motion, or eddy currents. The employment of nanoparticles smaller than 100 nm is especially advantageous in generating sufficient heat with low magnetic field strength. The heat generated by magnetic particles subject to an alternative magnetic field is suggested to be primarily size-dependent. As the particle size decreases, thermal activation of reorientation processes leads to superparamagnetic (SPM) behavior that is capable of generating impressive levels of heating at low field strengths when the Neel relaxation and Brownian motion are the dominant heating mechanisms (Fortin et al., 2008). The application of nanoparticles in magnetic hyperthermia offers a more effective treatment route than microparticles.

Subsequently, a targeted distribution of temperature elevation can be achieved by manipulating the particle distribution in the tumor and tuning the magnetic field parameters. Compared to most

conventional noninvasive heating approaches, this technique is capable of delivering adequate heat to tumor without necessitating heat penetration through the skin surface, thus avoiding the excessive collateral thermal damage along the path of energy penetration if the tumor is deep-seated. In addition to treatment of deep-seated tumor, the employment of nanoparticle smaller than 100 nm is especially advantageous in generating sufficient heating at a lower magnetic field strength. Typically, the particle dosage in the tumor and the magnetic field strength are carefully chosen to achieve the desired temperature elevation. Generally, the usable frequencies are in the range of 0.05 to 1.2 MHz and the field amplitude is controlled lower than 15 kA/m. Previous in vitro and in vivo studies have used a frequency in the hundred kilohertz range (Chan et al., 1993; Hase et al., 1989; Hilger et al., 2001; Jordan et al., 1997; Rand et al., 1981). The studies of heat generation by particles suggest that the heating characteristic of magnetic particles depends strongly on their properties, such as particle size, composition, and microstructure (Chan et al., 1993; Hergt et al., 2004; Hilger et al., 2001; Jordan et al., 1997). In particular, as the particle size decreases, thermal activation of reorientation processes leads to superparamagnetic (*SPM*) behavior that is capable of generating impressive levels of heating at lower field strengths. The spherical nanoparticle of 10 nm diameter is capable of providing a specific loss power (*SLP*) of 211 W/g under a magnetic field of 14 kA/m in amplitude and 300 kHz in frequency. In contrast, particles with diameter of 220 nm only generate an *SLP* of 144 W/g under identical a (Hilger et al., 2001). Experimental studies have been performed by Attaluri et al. (2011a, 2011b) on implanted PC3 tumors on mice, although it achieved similar temperature elevations in the tumors under a very low magnetic field strength (3 kA/m) (Attaluri et al., 2011a, 2011b). Magnetic nanoparticle hyperthermia has also been used to treat cancer in the kidney and skin (melanoma). A recent study by us has demonstrated the capability of elevating tumor temperature above 70°C using only 0.1 cc of a commercially available ferrofluid injected to PC3 tumor when it is subjected to a magnetic field strength (LeBrun et al., 2016a, 2016b). All of these studies have shown success in either moderate or complete thermal damage to various tumors using a wide range of strength of magnetic field with a frequency of several hundred kilohertz. Therefore, nanoparticle hyperthermia provides a more effective and clinically safer therapeutic alternative for cancer treatment than microparticles.

The quantification of heat generated by the particles has suggested that the size of the individual particle and properties of the magnetic field (strength and frequency) determine its heating capacity. Hence, given the particle size and magnetic field strength, it is the spatial distribution of the particle dispersed in tissue that affects the resulting temperature elevation. However, it is not clear how the spatial concentration of the particles in the tissue correlates with the particle concentration in the carrier solution before the injection. In nanofluid transport in tissue, the injection strategy as well as interaction between particle and the porous interstitial space may affect the particle distribution. An experimental study by our group has attempted to evaluate how to achieve a spherical shaped nanoparticle distribution in tissue. Figure 4.12 gives two images of nanoparticle distribution in agarose gel (0.2 percent) after a commercially available nanofluid was injected using a syringe pump. The selected injection rate affects significantly the final distribution of the nanofluid. As described in details in Salloum et al. (2008a), the ability of achieving a small spherical particle delivery is the first step to induce uniform temperature elevations in tumors with an irregular shape.

Depending on the amplitude of the magnetic field and particle dosage, the rate of temperature increase at the monitored site was as high as several degrees Celsius per minute. Temperatures up to 71°C were recorded at the tumor center (Hilger et al., 2005). The subsequent work by Johannsen and Jordan (Johannsen et al., 2005a, 2005b; Jordan et al., 2006) focused on testing the magnetic fluid hyperthermia on prostate cancer in human subjects. The histological analysis of the cancerous tissues showed a partial necrosis of the cells after the treatment. Recently, our group performed experimental study on the temperature elevation in rat muscle tissue induced by intramuscular injection of 0.2 cc nanofluid. The elevated temperatures were as high as 45°C and the FWHM (full length at half maximum) of the temperature elevation is 31 mm (Salloum et al., 2008b). All the experimental data have suggested the feasibility of elevating the tumor temperature to the desired level for tissue necrosis. However, in some tumor regions, usually at the tumor periphery, underdosage heating (temperature elevations lower than a critical value) was observed.

Laser photothermal therapy is another approach to maximally confine heat generation to targeted tumor region. It is an approach when metallic (gold) nanoparticles with a size much smaller than the

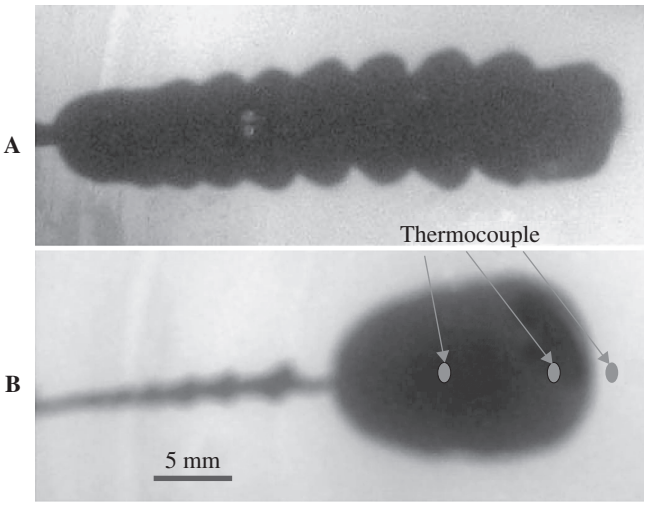

FIGURE 4.12 Two images of nanofluid distribution in agarose gel (0.2%). The injection rate was (A) 5 μL/min and (B) 2.5 μL/min, respectively. The nanofluid can be viewed by the black color in the images.

laser wavelength are exposed to laser irradiation at a specific laser wavelength near its plasmon resonant absorption band to activate and deactivate electrons, leading to dissipating energy. Specifically, laser has both electric and magnetic components, perpendicular to each other and perpendicular to the direction of energy and wave propagations. In the presence of an oscillating electromagnetic field of laser light, the conduction band of electrons of the metallic nanoparticle undergoes a collective coherent resonant oscillation with respect to surface plasmon oscillation. This requires that the natural frequency of the surface plasmon resonance (SPR) matches the frequency of the incident light; this phenomenon is called SPR. The frequency of SPR oscillation depends on the size, shape, surrounding medium, and dielectric constant of the nanoparticles (Huang et al., 2011). The induced surface plasmon oscillations decay either by radiative or nonradiative decay. In radiative decay the absorbed light energy causes phonon emission at the same frequency as the incident light, called Mie or Rayleigh scattering (Mie, 1908). This strong light scattering property of gold nanorods in the NIR region makes them potential candidates for noninvasive imaging techniques in the NIR band. The nonradiative decay occurs via electron-hole recombination. The energy exchange mechanism has two phases: electron–phonon interaction and phonon–phonon interaction. The excited electrons cool off rapidly by energy exchange with the nanoparticles in less than a picosecond, resulting in a hot particle lattice (Link and El-Sayed, 2000). The hot particle lattice exchanges this energy with the surrounding medium within 100 picoseconds via phonon–phonon interaction. The rapid energy exchange and strongly induced heat dissipation are desirable in hyperthermia applications.

The unique and easily tunable optical properties of gold nanoparticles with different shapes and structures such as nanospheres (Halas and West 2003; Hirsch et al., 2003), nanorods (Manuchehrabadi et al., 2012, 2013a, 2013b; Manuchehrabadi and Zhu, 2014), nanocages (Yavuz et al., 2009), nanoprism (Guo et al., 2010), nanowire (Heilmann and Kreibig, 2000), composite nanoparticles with core and shell structure (Kang and Taton, 2005), and nanoparticles with core and assemblies (Westcott et al., 1998) may confine laser energy to targeted tumors. Selecting a laser with appropriate wavelength is equally important. Laser photothermal therapy requires sufficient penetration of the laser energy through the superficial tissue and then adequate accumulation of laser absorption within the targeted tumor region. Among all the wavelengths of available lasers, the NIR range has the advantage of maximal transmissivity in normal tissue over other wavelengths. It has been suggested that an NIR laser with a wavelength of approximately 800 nm may penetrate into normal tissue with minimal laser absorption before reaching the targeted tumor with deposition of

gold nanorods. By carefully designing the size, shape, and structure of gold nanoparticles, one can achieve a desired absorption-scattering ratio in the therapeutic optical window (750 to 1100 nm) to maximize laser energy confinement in tumors (Myroshnychenko et al., 2008).

Previous experimental and theoretical studies have shown the effectiveness of laser photothermal therapy in cancer treatment both in tissue cultures and implanted tumors in mice (Manuchehrabadi et al., 2012). Successful treatment outcomes are illustrated by shrinkage of tumors following the therapy, as well as observed tumor cell death in tissue culture (Manuchehrabadi et al., 2013b).

Determination of SAR or Volumetric Heat Generation Rate q'''. SAR is a term normally used to describe heat generation rate per tissue mass. In heat conduction equation or the Pennes bioheat equation, the source term should carry a unit of watt per unit volume of tissue. Strictly speaking, one should convert SAR to q''' to be used in the heat transfer equation. Several methods are used to determine the q''' distribution induced by various heating applicators. The q''' distribution can be directly derived from the Maxwell equation of the electromagnetic field (Camart et al., 2000; Gentill et al., 1995; Ling et al., 1999; Stauffer et al., 1998; Strohbehn, 1984). The electrical field E and magnetic field B are first determined analytically or numerically from the Maxwell equation. The q''' is then calculated by the following equation (Sapozink et al., 1988):

$$q''' = \left(\frac{\sigma}{2\rho}\right)E^2 \tag{4.38}$$

where ρ and σ represent the density and conductivity of the media, respectively. This method is feasible when the derivation of the electromagnetic field is not very difficult. It generally requires a rather large computational resource and a long calculation time, though it is flexible for modeling the applicators and the surrounding media.

Other methods in clinical and engineering applications are experimental determination of the q''' distribution based on the heat conduction equation. The experiment is generally performed on a tissue equivalent phantom gel. The applicability of the q''' distribution measured in the phantom gel to that in tissue depends on the electrical properties of the phantom gel. For energy absorption of ultrasound in tissue, the gel mimics tissue in terms of ultrasonic speed and attenuation/absorption properties. For heat pattern induced by microwave or RF, the applicability requires that the phantom gel mimic the dielectric constant and electrical conductivity of the tissue. The electrical properties of various tissues at different wave frequencies have been studied by Stoy et al. (1982). It has been shown that in addition to the electromagnetic wave frequency, water content of the tissue is the most important factor determining the electrical properties. Thermal properties such as heat capacity and thermal conductivity of the gel are not required if no thermal study is conducted. The ingredients of the gel can be selected to achieve the same electrical characteristics of the tissue for a specific electromagnetic wavelength. As shown in Zhu and Xu (1998), the basic ingredients of the gel used for an RF heating applicator were water, formaldehyde solution, gelatin, and NaCl. Water was used to achieve a similar water content as the tissue. Formaldehyde and gelatin were the solidification agents. NaCl was added to obtain the desired electrical conductivity of tissue at that frequency. The resulted phantom gel was a semitransparent material that permits easy and precise positioning of the temperature sensors during the experimental study.

The simplest experimental approach to determining the q''' distribution is from the temperature transient at the instant of power on (Wong et al., 1993; Zhu et al., 1996b). In this approach, temperature sensors are placed at different spatial locations within the gel. Before the experiment, the gel is allowed to establish a uniform temperature distribution within the gel. As soon as the initial heating power level is applied, the gel temperature is elevated and the temperatures at all sensor locations are measured and recorded by a computer. The transient temperature field in the gel can be described by the heat conduction equation as follows:

$$\begin{aligned} \rho c\frac{\partial T}{\partial t} &= k\nabla^2 T + q'''(x,y,z) \\ t = 0, \qquad T &= T_{\text{env}} \end{aligned} \tag{4.39}$$

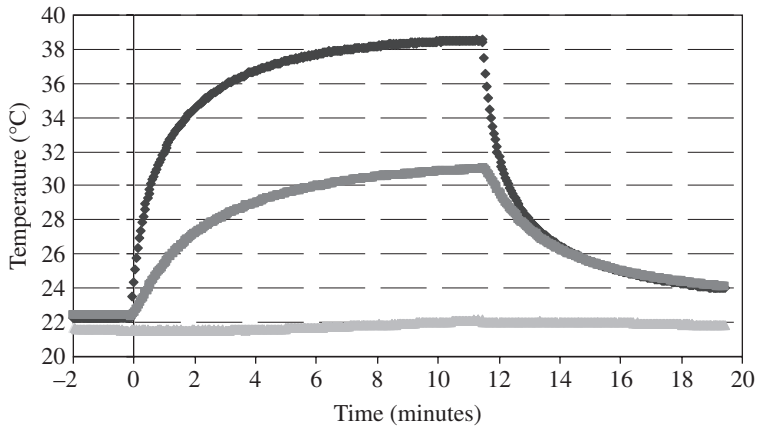

FIGURE 4.13 Initial temperature rises after heating is turned on. Temperatures are measured at three locations in the agarose gel, as shown in Fig. 4.12.

Within a very short period after the heating power is on, heat conduction can be negligible if the phantom gel is allowed to reach equilibration with the environment before the heating. Thus, q''' can be determined by the slope of the initial temperature rise at the specific location (x, y, z), i.e.,

$$q'''(x, y, z) = \rho c \left.\frac{\partial T(x, y, z, t)}{\partial t}\right|_{t=0} \tag{4.40}$$

Since q''' at each spatial location (x, y, z) is a constant during the heating, the temperature rise at each location is expected to increase linearly if heat conduction is negligible. Figure 4.13 gives the measured temperature rises at different radial locations from an injection site of the nanofluid. Note that the temperatures at all three probe locations were very close to each other before the heating. The temperatures increased linearly once the power was on; however, after approximately 60 seconds, the plot became curved and heat conduction within the gel was no longer negligible. For convenience the loose q''' data are generally represented by an analytic expression with several unknown parameters. Then a least-square residual fit of the q''' measurement to the analytical expression is performed to determine the unknown parameters in the expression.

It is simple to determine the q''' distribution from the initial temperature transient. This method is fairly accurate as long as the temperature is uniform before the power is turned on. However, to obtain an accurate expression for the q''' distribution, enough temperature sensors should be placed in the region where the energy is absorbed. In the situation when the SAR decays rapidly in the radial direction because of the superficial penetration of the energy, and it is difficult to place many temperature sensors in the near field, the q''' distribution must be determined by only a few measurements in the near field, which increases the measurement error.

In the experimental study by Zhu et al. (1998), the heating pattern induced by a microwave antenna was quantified by solving the inverse problem of heat conduction in a tissue equivalent gel. In this approach, detailed temperature distribution in the gel is required and predicted by solving a two-dimensional or three-dimensional heat conduction equation in the gel. In the experimental study, all the temperature probes were not required to be placed in the near field of the catheter. Experiments were first performed in the gel to measure the temperature elevation induced by the applicator, as shown in Fig. 4.14. An expression with several unknown parameters was proposed for the q''' distribution. Then, a theoretical heat transfer model was developed with appropriate boundary conditions and initial condition of the experiment to study the temperature distribution in the gel. The values of those unknown parameters in the proposed q''' expression were initially assumed and the temperature field in the gel was calculated by the model. The parameters were then adjusted to minimize the square error of the deviations of the theoretically predicted from the experimentally measured temperatures at all temperature sensor locations.

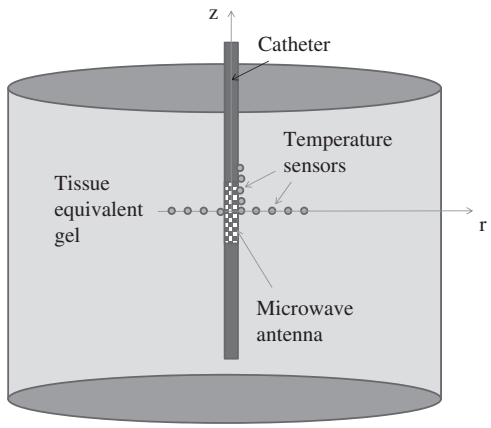

FIGURE 4.14 Schematic diagram of an experimental set up for measuring SARs at various tissue-equivalent phantom locations for microwave-induced heating.

4.5.4 Dynamic Response of Blood Flow to Hyperthermia

As mentioned previously, blood flow plays a profound effect in the temperature field during hyperthermia treatment. Accurately measuring and monitoring blood flow in different tissue regions and at different heating levels are especially crucial to achieve the thermal goal. The distribution of blood flow is quite heterogeneous in the tissue. Blood flow rate may be higher in the skin than in the muscle. Blood flow in the tumor and normal tissue may also be quite different because of different vasculatures. Contrary to the general notion that blood flow is less in tumors than in normal tissues, blood flow in many tumors, particularly in small tumors, is actually greater than that in surrounding normal tissues at normothermic conditions. Even in the same tumor, blood flow generally decreases as the tumor grows larger, owing partially to progressive deterioration of vascular beds and to the rapid growth of tumor cell population relative to vascular bed.

The dynamic responses of the blood flow to hyperthermia in normal tissue and tumors are even more diversified than the blood flow heterogeneity. It is a well-known fact that heat induces a prompt increase in blood flow accompanied by dilation of vessels and an increase in permeability of the vascular wall in normal tissues. The degree of pathophysiological changes in the vascular system in normal tissue is, of course, dependent on the heating temperature, the heating duration, and the heating protocol. Experimental study by Song (1984) has shown how the vasculature changed in the skin and muscle of rodents at different time intervals after hyperthermia for varying heating temperatures at 42° to 45°C. It was shown that the blood flow in the skin increased by a factor of 4 and 6 upon heating at 43°C for 60 and 120 minutes, respectively. At 44°C the skin blood flow was about 12 times the control value within 30 minutes. At high heating temperature, there existed a critical time after which the blood flow decreased because of vasculature damage. This critical time was more quickly reached when the heating temperature was higher. The blood flow increase in the muscle was similar to that observed in the skin layer, a tenfold increase in the blood flow was noticed at the 45°C heating.

An indisputable fact emerging from various experimental data indicates that heat-induced change in the blood flow in some tumors is considerably different from that in normal tissue. As noted in Fig. 4.15, there was a limited increase in blood flow in tumors during the initial heating period (Song, 1984). When the heating was prolonged, the tumor blood flow decreased progressively. The different responses of the normal tissue and tumors suggest the feasibility of selective tumor heating. A relatively small increase in blood flow in tumors favors retention of heat within the tumor volume, and thus causes greater heat damage. On the other hand, a large blood flow increase in the normal tissue by vascular dilation causes tissue cooling and high survival of cells.

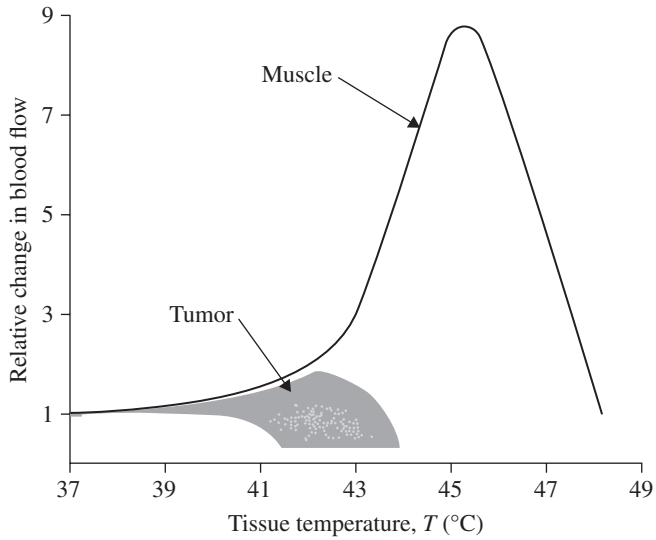

FIGURE 4.15 Temperature-dependent changes in the relative blood perfusion rates for muscle and animal tumors. [*From Song (1984) with permission.*]

Since blood flow is the major route of heat dissipation during hyperthermia, attempts have been made to modify the vascular responses in tumors and normal tissue to heat (Reinhold and Endrich, 1986; Song, 1991). Decreased tumor perfusion may induce changes in the tumor microenvironment, such as reduced pH value and energy supply, thus enhance the thermal cytotoxicity (Gerweck, 1977; Overgaard, 1976; Song et al., 1994). An injection of hydralazine to dogs was reported to decrease the blood flow by 50 percent in the tumor and increase the blood flow in the underlying muscle by a factor of three (Song, 1984). It was demonstrated that the use of vasoactive drugs led to intracellular acidification of the tumor environment (Song et al., 1994). It has been shown that 1 hour after an intravenous or intraperitoneal injection of KB-R8498, the blood flow in the SCK mammary carcinoma tumors of mice was reduced 30 to 60 percent (Griffin et al., 1998; Ohashi et al., 1998). The effect has also been made to induce a blood flow increase in the normal tissue. It was reported that preferentially dilating vessels in normal tissues using vasodilator such as sodium nitroprusside led to shunting of blood away from the tumor, and thus reducing the cooling effect of the blood flow in a tumor during local hyperthermia (Jirtle, 1988; Prescott et al., 1992). Not surprisingly, radiation also altered the response of vasculatures to heat. It was reported that irradiation with 2000 R given 1 hour before heating at 42°C for 30 minutes enhanced the heat-induced vascular damage in the cervical carcinoma of hamsters. Another research showed that hyperthermia of 42°C for 1 hour, given several weeks after irradiation, enhanced the capacity of blood flow increase in skin and muscle (Song, 1984).

It has been increasingly evident that the response of vascular beds to heat in tumors differs considerably from that in normal tissues. The effective clinical use of hyperthermia depends on a careful application of these biological principles emerging from experimental work. More experimental measurements of temperature response are needed for different tumor types at different ages. It is also important to evaluate the applicability of the dynamic response measured in animal to human subjects. Another issue to be addressed is the hyperthermia-induced blood flow change in drug delivery, since the reduced tumor blood flow may decrease the drug delivered to the tumors.

4.5.5 Assessment of Thermal Damage

An optimal heating protocol for a heating experiment can be determined based on the Arrhenius integral or the EM_{43}, an alternative parameter derived from the Arrhenius integral (Dewhirst et al., 2003;

Moritz and Henriques, 1947; Sapareto and Dewey, 1984). The Arrhenius integral (Moritz and Henriques, 1947) can be used to quantitatively assess thermal damage based on measured or simulated temperature history at various tissue locations. Damage is considered to be a unimolecular process. In this process, the native molecules are transformed into a coagulated state, leading to cell death. Damage is quantified as a single dimensionless parameter Ω. This equation is referred to as the Arrhenius integral as follows:

$$\Omega(x, y, z, \tau) = \ln\left[\frac{C(0)}{C(\tau)}\right] = A\int_0^{\tau} \exp\left[-\frac{E_a}{R_u T(x, y, z, t)}\right]dt \tag{4.41}$$

where t is time, C is the concentration of undamaged cells, A is the preexponential factor or frequency factor (1/s), E_a is the activation energy barrier (J/mole), R_u is the universal gas constant (J/mole·K), and $T(x, y, z, t)$ is the absolute tissue temperature at the location (x, y, z). Ω, the extent of damage, is defined as the logarithm of the ratio of the initial concentration of the healthy cells, $C(0)$, to the concentration of the healthy cells remaining after thermal treatment, $C(\tau)$, for a duration of τ. The value of Ω is zero before any thermal therapy, and it increases during heating. Sixty-three percent and 98.2 percent denaturation of protein occurs when $\Omega = 1$ and 4, respectively (LeBrun et al., 2016b). Note that Ω is a function of both tissue location (x, y, z) and heating time τ. Implementing the integral requires knowing of the activation energy and the frequency factor associated with the tissue cells. The values of E_a and A are determined by inverse thermal analyses in matching the model to the data for cell injury and temperature-time history of exposure. The activation energy and frequency factor are related to activation enthalpy and entropy. From the exponential nature of the equation, it suggests that rate damage accumulation will be negligible below certain temperature threshold. Once the threshold value is exceeded, a swift increase in the rate damage accumulation is expected.

The Arrhenius parameters A and E_a are both temperature and cell line/tissue dependent and are typically determined using inverse heat transfer analysis. One previous study of thermal tolerance of various carcinoma cells demonstrated that human prostatic carcinoma cell lines are much easier to be damaged than carcinoma cell lines of other human origins such as colon, breast, lung, and brain under the same mild hyperthermia dosage (Ryu et al., 1996). For example, PC3 cells and RWPE-1 (prostate cells) in the thermal ablation region have frequency factor of is $7 * 10^{17}$ 1/s and the $5.65 * 10^{7}$ 1/s and an activation energy of $1.25 * 10^{5}$ J/mol and $5.88 * 10^{4}$ J/mol, respectively (Rylander et al., 2006). Recently, the Arrhenius integral $\Omega = 4$ is used to design heating time for 100 percent damaging PC3 tumors implanted on mice (LeBrun et al., 2016a). Based on the nanoparticle distribution in a tumor obtained from microCT scans and imported to COMSOL (LeBrun et al., 2016a), one simulates the temperature transients in the tumor, and the heating time of 25 minutes is identified to satisfy the minimal Ω value of 4 over the entire tumor. The Arrhenius damage model is still being used extensively in the field of hyperthermia as a means to predict the probability of damage.

In clinical studies for specific type of cancers and growth stage, it is a common practice to perform experiments at 43°C to determine how long it will take to induce cell damage to a cell of specific type and growth stage. This method is referred to as the cumulative effective minutes at 43°C or CEM_{43}. CEM_{43}, the thermal isoeffective dose, converts the temperature levels and heating duration into an equivalent number of minutes at 43°C to induce the necessary thermal damage. CEM_{43} is widely used to evaluate thermal damage to cells previously studied to understand whether the designed treatment protocols achieve the same thermal dosage. CEM_{43} has been extensively and successfully used in clinical trials to assess the efficacy of heating, despite the fact that the R value has been historically derived from cell cultures and rodents (Nadobny et al., 2015). The proposed method for estimating damage using this method is given as

$$\text{CEM}_{43} \text{ for } T_i = \sum_{j=1}^{n} \Delta t_j R^{T_i(t_j)-43} \tag{4.42}$$

where T_i is the temperature at location i and Δt is the time at T_i. A more general expression of EM43 can be written as

$$\text{CEM}_{43} \text{ for location } i = \int_0^{t} R^{T_i(t)-43} dt \tag{4.43}$$

The parameter R is referred to the R-value and it represents a constant that is dependent on the temperature range (Dewhirst et al., 2003; Manuchehrabadi et al., 2013). Similar to the Arrhenius model, R-value is cell line/tissue dependent. Typical R-values for human prostate cancer (PC3) with their temperature ranges can be as follows:

$$R = \begin{cases} 4 & T < 43°\text{C} \\ 2 & 48°\text{C} \geq T \geq 43°\text{C} \\ 1.33 & T > 48°\text{C} \end{cases} \tag{4.44}$$

CEM_{43} method suggests that if temperatures are higher than 43°C, the treatment time decreases. When the tissue temperature is higher than 43°C, the equivalent minutes at 43°C is longer than the actual heating time. For example, if the temperature is maintained at 46°C (R-value of 2) for 20 minutes, i.e., $\Delta t_j = 20$, the equivalent minutes for this time segment will be $20 * 2^{46\text{-}43} = 320$ minutes at 43°C. In other words, the equivalent minutes can be much higher than the actual heating time when the tumor temperature is higher than 43°C. If the calculated number of equivalent minutes is longer than the CEM_{43}, thermal damage is ensured. One study using ultrasound heating determined that the critical thermal dose for liver tissue is $CEM_{43} = 340$ minutes when temperatures are maintained at 54°C (Graham et al., 1999). A recent study by Manuchehrabadi et al. (2013b) has used the approach to estimate the CEM43 in PC3 tumors implanted in mice. The heating is induced by an 808-nm laser with a heating duration of 15 minutes. Based on the measured temperature mapping along two tumor paths in an in vivo experiment, one estimates the EM43 values at all the measurement locations. More than 93 percent of the locations have a CEM43 value longer than 110 minutes. Later the results are compared to histologic analyses and tumor shrinkage studies after the same treatment protocol. The distribution of thermal damage observed in the experiment agrees with the theoretical prediction of the CEM_{43} values.

4.5.6 Theoretical Modeling

In treatment planning, quantitative three-dimensional thermal modeling aids in the identification of power delivery for optimum treatment. Thermal modeling provides the clinician with powerful tools that improve the ability to deliver safe and effective therapy, and permits the identification of critical monitoring sites to assess tumor heating as well as to assure patient safety. Thermal modeling maximizes the information content of (necessarily sparse) invasive thermometry. The empirical temperature expression (if it is possible) can be used to develop an online reference for monitoring tissue temperatures and building a feedback control of the applied power to avoid overheatings in critical tissue areas during the hyperthermia therapy.

Tissue temperature distributions during hyperthermia treatments can be theoretically determined by solving the bioheat transfer equation (continuum model or vascular model), which considers the contributions of heat conduction, blood perfusion, and external heating. In addition to geometrical parameters and thermal properties, the following knowledge must be determined before the simulation. The SAR distribution induced by the external heating device should be determined first. The regional blood perfusion in the tissue and tumor and their dynamic responses to heating are also required. All this information, with appropriate boundary and initial conditions allows one to calculate the temperature distribution of the tissue.

Analytical solution for the temperature field during the hyperthermia treatment is available for certain tissue geometries (Liu et al., 2000; Zhu and Xu, 1999). In most of the situations, temperature field is solved by numerical methods because of the irregular tissue geometry and complicated dynamic response of blood flow to heating (Charny et al., 1987; Chatterjee and Adams, 1994; Clegg and Roamer, 1993; Zhu et al., 2009a, 2009b).

Unfortunately, the distribution of the volumetric heat generation rate in tumors induced by a specific heating method is often nonuniform and unknown. Most tumors are also not represented correctly using simple geometries. These challenges may be addressed by proposing theoretical modeling based on realistic tumor model and volumetric heat generation rate distribution obtained from imaging scans after calibrations. With the advancement of computational and storage resources in the past decade, modeling biotransport in tissue is no longer implemented in simplified geometries such as rectangular

columns, cylinders, and spheres. For example, in laser photothermal therapy or laser treatment, traditional approach is to use 1D Beer's law or a modified Beer's law that combines absorption and scattering into a single extinction coefficient to address energy absorption. Currently, energy absorption in tumors by laser can be easily modeled using Monte Carlo simulation that is sufficiently flexible to handle complex geometrical shapes, anisotropic scattering, and nonhomogeneous properties. This method assumes laser as photons emitted from a laser source (Manuchehrabadi et al., 2013a). After a single photon is incident on a tissue surface, the photon can either be specularly reflected or continue to transport inside the tissue. At each step the photon travels, the direction in which it will be heading to and how much energy dissipation due to absorption when the photon interacts with the tissue are determined by probability functions. In addition, photons can interact with tissue via scattering from a particle or tiny tissue structure. During scattering, several probability functions are used to determine which direction the photon will bend from its original path based on an anisotropic factor, as well as the length of the next step of the photon after scattering. After a series of scattering and absorption events inside the tissue, the photons may exhaust their energy to zero or escape from the tissue region. Monte Carlo simulations usually require emitting thousands of photons onto the tissue surface, based on the laser irradiation distribution. This long simulation-intensive process has been shortened significantly due to advancement in computational resources. Any energy dissipation due to absorption in a unit volume element can then be added to calculate the total energy absorption rate by the element to determine the volumetric heat generation rate distribution in tissue, to be used in bioheat transfer simulation.

In magnetic nanoparticle hyperthermia, the available computational resource in recent years makes it possible to import the acquired 3D images of tumor geometries and detailed nanoparticle concentration distribution to commercial software packages for accurate heat transfer simulation. A heat transfer model based on image-generated tumor geometry and volumetric heat generation rate distribution would greatly improve model predicting power and lead to individualized and reliable treatment designs for various tumor sizes and types (LeBrun et al., 2016a). As shown in Fig. 4.16, a prototype

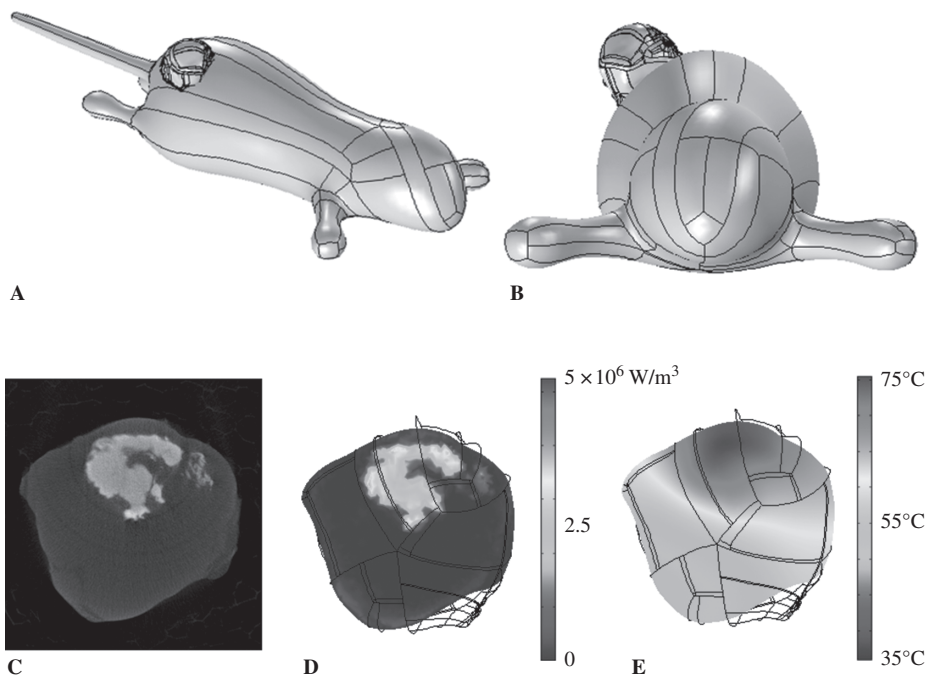

FIGURE 4.16 Generated tumor model embedded in a mouse body from microCT scans (A and B); a slice of microCT image of a tumor with nanoparticle injection (C); generated color contours of volumetric heat generation rate in COMSOL (D); and simulated temperature distribution in the tumor during steady state (E).

of a tumor from about 500 microCT scan slices is generated and mounted on a prototype of a mouse body. Also illustrated in Fig. 4.16 are: an original microCT scan slice of the tumor, an imported volumetric heat generation rate contour to COMSOL, and the resulted steady-state temperature elevation distribution in the tumor (LeBrun et al., 2016a). It is an important advancement to accurately model the details in those geometries and the resulted volumetric heat generation rate distribution, especially when point-to-point comparisons are necessary in some future theoretical simulation applications.

Parametric studies can be performed to evaluate the influence of different parameters, such as heating level, tissue perfusion, and cooling fluid, on the temperature elevation. Extensive parametric studies can be performed quickly and inexpensively so that sensitive (and insensitive) parameters can be identified, systems can be evaluated, and critical experiments can be identified. This is especially important when the parameter is unknown. It is also possible to extract the ideal SAR distribution from the parametric study (Loulou and Scott, 2000) and design an improved heating applicator in future. Knowledge of the expected thermal profiles could be used to guide experimental and clinical studies in using an optimum thermal dose to achieve a desired therapeutic effect. The optimal thermal dose needed in the treatment volume predicted by the theory helps physicians to evaluate the effectiveness of the heating devices and their treatment protocols.

4.6 CONCLUSION

Building on previous efforts to understand fundamental roles played by vasculature on temperature field in biological systems, bioengineers have greatly improved their ability of modeling temperature fields in tissue with high precision for treatment planning with the advancements in computational resources and newly developed imaging tools, which allow accurate description of the tissue geometry and heating source/sink distribution. This greatly enhances the simulation accuracy of heat and mass transfer processes in tissue, which are critical for generating an optimal temperature distribution to achieve the clinical objectives. Hyperthermia treatments using newly developed nanostructures have the advantage over traditional heating approaches via providing confined heat generation in the targeted tumor region. High-resolution imaging systems and multiscale modeling have tremendous potential for gaining insight into contributions of various transport mechanisms in nanostructure transport and distribution in tumors during both hyperthermia treatments and therapeutic agent delivery to targeted tissue region. The challenges facing engineers are how to include dynamic responses of local blood perfusion, changes in transport properties in tumors, and volumetric heat generation rate redistribution during a heating process into theoretical simulations to better design treatment protocols and/or adjust treatment protocol based on real-time monitoring of those dynamic parameters.

ACKNOWLEDGMENT

This review was supported by an NSF research grant (CBET-1705538).

REFERENCES

Arkin, H., Holmes, K. R., and Chen, M. M., 1987, "Computer Based System for Continuous On-line Measurements of Tissue Blood Perfusion," *Journal of Biomedical Engineering*, **9**:38–45.

Arkin, H., Holmes, K. R., Chen, M. M., and Bottje, W. G., 1986, "Thermal Pulse Decay Method for Simultaneous Measurement of Local Thermal Conductivity and Blood Perfusion: A Theoretical Analysis," *ASME Journal of Biomechanical Engineering*, **108**:208–214.

Astrahan, M. A., and Norman, A., 1982, "A Localized Current Field Hyperthermia System for Use with 192 Iridium Interstitial Implants," *Medical Physics*, **9**:419–424.

Attaluri, A., Ma, R., Qiu, Y., Li, W., and Zhu, L., 2011a, "Nanoparticle Distribution and Temperature Elevations in Prostatic Tumors in Mice during Magnetic Nanoparticle Hyperthermia," *International Journal of Hyperthermia*, **27**(5):491–502.

Attaluri, A., Ma, R., and Zhu, L., 2011b, "Using MicroCT Imaging Technique to Quantify Heat Generation Distribution Induced by Magnetic Nanoparticles for Cancer Treatments," *ASME Journal of Heat Transfer*, **133**(1):011003(1–5).

Aurer, C., and Carpenter, D. O., 1980, "Choroidal Blood Flow as a Heat Dissipating Mechanism in the Macula," *American Journal of Ophthalmology*, **89**:641–646.

Baish, J. W., 1994, "Formulation of a Statistical Model of Heat Transfer in Perfused Tissue," *ASME Journal of Biomechanical Engineering*, **116**:521–527.

Banerjee, R. K., Zhu, L., Gopalakrishnan, P., and Kazmierczak, M. J., 2007, "Influence of Laser Parameters on Selective Retinal Treatment Using Single-Phase Heat Transfer Analyses," *Medical Physics*, **34**(5):1828–1841.

Barberia, E., Maroto, M., Arenas, M., and Silva, C. C., 2008, "A Clinical Study of Caries Diagnosis with a Laser Fluorescence System," *Journal of the American Dental Association,* **139**:572–579.

Bartgis, C., LeBrun, A., Ma, R., and Zhu, L., 2016, "Determination of Time of Death in Forensic Science via a 3-D Whole Body Heat Transfer Model," *Journal of Thermal Biology*, **62**:109–115.

Bazett, H. C., 1941, "Temperature Sense in Men," in *Temperature: Its Measurement and Control in Science and Industry*, New York: Reinhold, pp. 489–501.

Bernard, V., Staffa, E., Mornstein, V., and Bourek, A., 2013, "Infrared Camera Assessment of Skin Surface Temperature—Effect of Emissivity," *Physica Medica*, **29**:583–591.

Borgos, J., 1996, "Laser Doppler Monitoring of Cerebral Blood Flow," *Neurological Research*, **18**:251–255.

Brinck, H., and Werner, J., 1994, "Estimation of the Thermal Effect of Blood Flow in a Branching Countercurrent Network Using a Three-dimensional Vascular Model," *ASME Journal of Biomechanical Engineering*, **116**:324–330.

Camart, J. C., Despretz, D., Prevost, B., Sozanski, J. P., Chive, M., and Pribetich, J., 2000, "New 434 MHz Interstitial Hyperthermia System Monitored by Microwave Radiometry: Theoretical and Experimental Results," *International Journal of Hyperthermia*, **16**:95–111.

Cetas, T. C., Conner, W. G., and Manning, M. R., 1980, "Monitoring of Tissue Temperature During Hyperthermia Therapy," *Annals of the New York Academy of Sciences*, **335**:281–297.

Chan, D. C. F., Kirpotin, D. B., and Bunn, P. A., 1993, "Synthesis and Evaluation of Colloidal Magnetic Iron Oxides for the Site-specific Radio Frequency-induced Hyperthermia of Cancer," *Journal of Magnetism and Magnetic Materials,* **122**:374–378.

Charny, C. K., Hagmann, M. J., and Levin, R. L., 1987, "A Whole Body Thermal Model of Man during Hyperthermia," *IEEE Transactions on Biomedical Engineering*, **34**(5):375–387.

Charny, C. K., Weinbaum, S., and Levin, R. L., 1990, "An Evaluation of the Weinbaum-Jiji Bioheat Equation for Normal and Hyperthermic Conditions," *ASME Journal of Biomechanical Engineering*, **112**:80–87.

Chato, J. 1980, "Heat Transfer to Blood Vessels," *ASME Journal of Biomechanical Engineering*, **102**:110–118.

Chatterjee, I., and Adams, R. E., 1994, "Finite Element Thermal Modeling of the Human Body under Hyperthermia Treatment for Cancer," *International Journal of Computer Applications in Technology*, **7**:151–159.

Chaussy, C., and Thuroff, S., 2001, "Results and Side Effects of High-Intensity Focused Ultrasound in Localized Prostate Cancer," *Journal of Endourology,* **15**:437–440.

Chen, M. M., and Holmes, K. R., 1980, "Microvascular Contributions to Tissue Heat Transfer," *Annals of the New York Academy of Science*, **335**:137–150.

Chu, C. H., Lo, E. C. M., and You, D. S. H., 2010, "Clinical Diagnosis of Fissure Caries with Conventional and Laser-Induced Fluorescence Techniques," *Lasers in Medical Science,* **25**:355–362.

Clark, R. S., Kochanek, P. M., Marion, D. W., Schiding, J. K., White, M., Palmer, A. M., and DeKosky, S. T., 1996, "Mild Posttraumatic Hypothermia Reduces Mortality after Severe Controlled Cortical Impact in Rats," *Journal of Cerebral Blood Flow and Metabolism,* **16**(2):253–261.

Clegg, S. T., and R. B. Roemer, 1993, "Reconstruction of Experimental Hyperthermia Temperature Distributions: Application of State and Parameter Estimation," *ASME Journal of Biomechanical Engineering*, **115**:380–388.

Cosset, J. M., Dutreix, J., Haie, C., Mabire, J. P., and Damia, E., 1986, "Technical Aspects of Interstitial Hyperthermia," in *Recent Results in Cancer Research*, Vol. 101, Berlin, Heidelberg: Springer, pp. 56–60.

Crezee, J., and Lagendijk, J. J. W., 1990, "Experimental Verification of Bioheat Transfer Theories: Measurement of Temperature Profiles Around Large Artificial Vessels in Perfused Tissue," *Physics in Medicine and Biology*, **35**(7):905–923.

Crezee, J., Mooibroek, J., Bos, C. K., and Lagendijk, J. J. W., 1991, "Interstitial Heating: Experiments in Artificially Perfused Bovine Tongues," *Physics in Medicine and Biology*, **36**:823–833.

Devarakonda, S., Bulusu, P., Al-Rjoub, M. F., Bhattacharya, A., and Banerjee, R. K., 2018, "Influence of External Head Cooling on the Head, Core Body, and Blood Temperatures Using 3D Whole Body Model," *International Journal of Numerical Methods for Heat and Fluid Flow*, **28**(10):2491–2504.

Dewhirst, M. W., Prosnitz, L., Thrall, D., Prescott, D., Clegg, S., Charles, C., MacFall, J., Rosner, G., Samulski, T., Gillette, E., and LaRue, S., 1997, "Hyperthermia Treatment of Malignant Diseases: Current Status and a View Toward the Future," *Seminars in Oncology*, **24**(6):616–625.

Dewhirst, M. W., Viglianti, B. L., Lora-Michiels, M., Hanson, M., and Hoopes, P. J., 2003, "Basic Principles of Thermal Dosimetry and Thermal Thresholds for Tissue Damage from Hyperthermia," *International Journal of Hyperthermia*, **19**(3):267–294.

Dorr, L. N., and Hynynen, K., 1992, "The Effects of Tissue Heterogeneities and Large Blood Vessels on the Thermal Exposure Induced by Short High-power Ultrasound Pulses," *International Journal of Hyperthermia*, **8**:45–59.

Engelhart, M., and Kristensen, J. K., 1986, "Raynaud's Phenomenon: Blood Supply to Fingers During Indirect Cooling, Evaluated by Laser Doppler Flowmetry," *Clinical Physiology*, **6**:481–488.

Firorini, A., Fumero, R., and Marchesi, R., 1983, "Cardio-surgical Thermography," *Proceedings of SPIE*, **359**:249.

Flower, R. W., 2002, "Optimizing Treatment of Choroidal Neovascularization Feeder Vessels Associated with Age-Related Macular Degeneration," *American Journal of Ophthalmology*, **134**:228–239.

Fortin, J. P., Gazeau, F., and Wilhelm, C., 2008, "Intracellular Heating of Living Cells through Néel Relaxation of Magnetic Nanoparticles," *European Biophysics Journal,* **37**(2):223–228.

Fu, G., 1995, "A Transient 3-D Mathematical Thermal Model for the Clothed Human," Ph.D. Dissertation, Kansas State University.

Gautherie, M., and Gros, C. M., 1980, "Breast Thermography and Cancer Risk Prediction," *Cancer*, **45**(1):51–56.

Gelet, A., Chapelon, J. Y., Bouvier, R., Rouviere, O., Lyonnet, D., and Dubernard, J. M., 2001, "Transrectal High Intensity Focused Ultrasound for the Treatment of Localized Prostate Cancer: Factors Influencing the Outcome," *European Urology*, **40**:124–129.

Gentill, G. B., Lenocini, M., Trembly, B. S., Schweizer, S. E., 1995, "FDTD Electromagnetic and Thermal Analysis of Interstitial Hyperthermic Applicators: Finite-difference Time-domain," *IEEE Transactions on Biomedical Engineering*, **42**(10):973–980.

Gerweck, L. E., 1977, "Modification of Cell Lethality at Elevated Temperatures: the pH Effect," *Radiation Research*, **70**:224–235.

Gilchrist, R. K., Medal, R., Shorey, W. D., Hanselman, R. C., Parrott, J. C., and Taylor, C. B., 1957, "Selective Inductive Heating of Lymph Nodes," *Annals of Surgery*, **146**:596–606.

Graham, S. J., Chen, L., Leitch, M., Peters, R. D., Bronskill, M. J., Foster, F. S., Henkelman, R. M., and Plewes, D. B., 1999, "Quantifying Tissue Damage due to Focused Ultrasound Heating Observed by MRI," *Magnetic Resonance in Medicine*, **41**(2):321–328.

Griffin, R. J., Ogawa, A., Shakil, A., and Song, C. W., 1998, "Local Hyperthermia Treatment of Solid Tumors: Interplay between Thermal Dose and Physiological Parameters," ASME, HTD-Vol. 362, *Advances in Heat and Mass Transfer in Biological Systems*, pp. 67–69.

Guo, Z., Fan, X., Liu, L., Bian, Z., Gu, C., Zhang, Y., Gu, N., Yang, D., and Zhang, J., 2010, "Achieving High-purity Colloidal Gold Nanoprisms and Their Application as Biosensing Platforms," *Journal of Colloid and Interface Science,* **348**(1):29–36.

Halas, N. J., and West, J. L., 2003, "Nanoshell-Mediated Near-Infrared Thermal Therapy of Tumors under Magnetic Resonance Guidance," *Proceedings of the National Academy of Sciences*, **100**(23):13549–13554.

Hariharan, P., Chang, I, Myers, M., and Banerjee, R. K., 2007a, "Radio Frequency (RF) Ablation in a Realistic Reconstructed Hepatic Tissue," *ASME Journal of Biomechanical Engineering*, **129**:354–364.

Hariharan, P., Myers, M. R., and Banerjee, R. K., 2007b, "HIFU Procedures at Moderate Intensities—Effect of Large Blood Vessels," *Physics in Medicine & Biology*, **52**:3493–3513.

Hartov, A., Colacchio, T. A., Hoopes, P. J., and Strohbehn, J. W., 1994, "The Control Problem in Hyperthermia," ASME HTD-Vol. 288, *Advances in Heat and Mass Transfer in Biological Systems*, pp. 119–126.

Hase, M., Sako, M., Fujii, M., Ueda, E., Nagae, T., Shimizu, T., Hirota, S., and Kono, M., 1989, "Experimental Study of Embolohyperthermia for the Treatment of Liver Tumors by Induction Heating to Ferromagnetic Particles Injected into Tumor Tissue," *Nippon Acta Radiologica,* **49**:1171–1173.

He, Q., Zhu, L., and Weinbaum, S., 2003, "Effect of Blood Flow on Thermal Equilibration and Venous Rewarming," *Annals of Biomedical Engineering*. **31**:659–666.

He, Q., Zhu, L., Weinbaum, S., and Lemons, D. E., 2002, "Experimental Measurements of Temperature Variations along Paired Vessels from 200 to 1000 μm In Diameter in Rat Hind Leg," *ASME Journal of Biomedical Engineering*, **124**:656–661.

Head, J. F., Wang, F., and Elliott R. L., 1993, "Breast Thermography Is a Noninvasive Prognostic Procedure That Predicts Tumor Growth Rate in Breast Cancer Patients," *Annals of New York Academy of Sciences*, **698**:153–158.

Heilmann, A., and Kreibig, U., 2000, "Optical Properties of Embedded Metal Nanoparticles at Low Temperatures," *European Physical Journal Applied Physics*, **10**(3):193–202.

Hergt, R., Hiergeist, R., Zeisberger, M., Glockl, G., Weitschies, W., Ramirez, L. P., Hilger, I., and Kaiser, W. A., 2004, "Enhancement of AC-losses of Magnetic Nanoparticles for Heating Applications," *Journal of Magnetism and Magnetic Materials*, **280**:358–368.

Hilger, I., Andra, W., Hergt, R., Hiergeist, R., Schubert, H., and Kaiser, W. A., 2001, "Electromagnetic Heating of Breast Tumors in Interventional Radiology: In Vitro and In Vivo Studies in Human Cadavers and Mice," *Radiology*, **218**:570–575.

Hilger, I., Hergt, R., and Kaiser, W. A., 2005, "Towards Breast Cancer Treatment by Magnetic Heating," *Journal of Magnetism and Magnetic Materials*, **293**:314–319.

Hirsch, L. R., Stafford, R. J., Bankson, J. A., Sershen, S. R., Rivera, B., Price, R. E., Hazle, J. D., and Holmes, K. R., 1997, "Biological Structures and Heat Transfer," in *Report from the Allerton Workshop on the Future of Biothermal Engineering*, pp.14–37.

Hu, L., Gupta, A., Gore, J. P., and Xu, L. X., 2004, "Effect of Forced Convection on the Skin Thermal Expression of Breast Cancer," *Journal of Biomechanical Engineering*, **126**(2):204–211.

Huang, S. K., Bharati, S., Graham, A. R., Lev, M., Marcus, F. I., and Odell, R. C., 1987, "Closed Chest Catheter Desiccation of the Atrioventricular Junction Using Radiofrequency Energy — A New Method of Catheter Ablation," *Journal of the American College of Cardiology*, **9**:349–358.

Huang, X., Jiang, P., and Tanaka, T., 2011, "A Review of Dielectric Polymer Composites with High Thermal Conductivity," *IEEE Electrical Insulation Magazine*, **27**(4):8–16.

Huikeshoven, M., Koster, P. H., de Borgie, C. A., Beek, J. F., van Gemert, M. J., and van der Horst, C. M., 2007, "Redarkening of Port-Wine Stains 10 Years After Pulsed-Dye-Laser Treatment," *New England Journal of Medicine*, **356**(12):1235–1240.

Izikson, L., Nelson, J. S., and Anderson, R. R., 2009, "Treatment of Hypertrophic and Resistant Port Wine Stains with a 755 nm Laser: A Case Series of 20 Patients," *Lasers in Surgery and Medicine*, **41**(6):427–432.

Jamieson, S. W., Kapelanski, D. P., Sakakibara, N., Manecke, G. R., Thistlethwaite, P. A., Kerr, K. M., Channick, R. N., Fedullo, P. F., and Auger, W. R., 2003, "Pulmonary Endarterectomy: Experience and Lessons Learned in 1,500 Cases," *Annals of Thoracic Surgery*, **76**(5):1457–1462.

Jasim, Z. F., and Handley, J. M., 2007, "Treatment of Pulsed Dye Laser Resistant Port Wine Stain Birthmarks," *Journal of American Academy of Dermatology*, **57**(4), 677–682.

Jia, W, Aguilar, G., Verkruysse, W., Franco, W., and Nelson, J. S., 2006, "Improvement of Port Wine Stain Laser Therapy by Skin Preheating Prior to Cryogen Spray Cooling: A Numerical Simulation," *Lasers in Surgery and Medicine*, **38**:155–162.

Jirtle, R. L., 1988, "Chemical Modification of Tumor Blood Flow," *International Journal of Hyperthermia*, **4**:355–371.

Johannsen, M., Gneveckow, U., Eckelt, L., Feussner, A., Waldofner, N., Scholz, R., Deger, S., Wust, P., Loening, S. A., and Jordan A., 2005a, "Clinical Hyperthermia of Prostate Cancer Using Magnetic Nanoparticles: Presentation of a New Interstitial Technique," *International Journal of Hyperthermia*, **21**:637–647.

Johannsen, M., Thiesen, B., Jordan, A., Taymoorian, K., Gneveckow, U., Waldofner, N., Scholz, R., Koch, M., Lein, M., Jung, K., and Loening, S. A., 2005b, "Magnetic Fluid Hyperthermia (MFH) Reduces Prostate Cancer Growth in the Orthotopic Dunning R3327 Rat Model," *Prostate*, **64**:283–292.

Jones, B. F., 1998, "A Reappraisal of the Use of Infrared Thermal Image Analysis in Medicine," *IEEE Transactions on Medical Imaging*, **17**(6):1019–1027.

Jordan, A., Scholz, R., Maier-Hauff, K., Van Landeghem, F. K., Waldoefner, N., Teichgraeber, U., Pinkernelle, J., Bruhn, H., Neumann, F., Thiesen, B., Von Deimling, A., and Felix, R., 2006, "The Effect of Thermotherapy Using Magnetic Nanoparticles on Rat Malignant Glioma," *Journal of Neuro-Oncology*, **78**:7–14.

Jordan, A., Scholz, R., Wust, P., Fahling, H., Krause, J., Wlodarczyk, W., Sander, B., Vogl, T., and Felix, R., 1997, "Effects of Magnetic Fluid Hyperthermia (MFH) on C3H Mammary Carcinoma in Vivo," *International Journal of Hyperthermia*, **13**(6):587–605.

Kalathil, R. T., D'Souza, G. A., Bhattacharya, A., and Banerjee, R. K., 2016, "Uncertainty Analysis of the Core Body Temperature Under Thermal and Physical Stress Using a Three-Dimensional Whole Body Model," *ASME Journal of Heat Transfer*, **139**:031102(1–10).

Kang, Y., and Taton, T. A., 2005, "Controlling Shell Thickness in Core−Shell Gold Nanoparticles via Surface-Templated Adsorption of Block Copolymer Surfactants," *Macromolecules*, **38**(14):6115–6121.

Kopyov, O., Jacques, D., Duma, C., Buckwalter, G., Kopyov, A., Lieberman, A., and Copcutt, B., 1997, "Microelectrode-guided Posteroventral Medial Radiofrequency Pallidotomy for Parkinson's Disease," *Journal of Neurosurgery*, **87**:52–55.

Lam, J. M. K., Hsiang, J. N. K., and Poon, W. S., 1997, "Monitoring of Autoregulation Using Laser Doppler Flowmetry in Patients with Head Injury," *Journal of Neurosurgery*, **86**:438–455.

Lanuti, M., Sharma, A., Digumarthy, S. R., Wright, C. D., Donahue, D. M., Wain, J. C., Mathisen, D. J., and Shepard, A. O., 2009, "Radiofrequency Ablation for Treatment of Medically Inoperable Stage I Non-small Cell Lung Cancer," *Journal of Thoracic and Cardiovascular Surgery*, **137**:160–166.

Lapayowker, M. S., and Revesz, G., 1980, "Thermography and Ultrasound in Detection and Diagnosis of Breast Cancer," *Cancer*, **46**(4 Suppl):933–938.

LeBrun, A., Ma, R., and Zhu, L., 2016a, "MicroCT Image Based Simulation to Design Heating Protocols in Magnetic Nanoparticle Hyperthermia for Cancer Treatment," *Journal of Thermal Biology*, **62**:129–137.

LeBrun, A., Joglekar, T., Bieberich, C., Ma, R., and Zhu, L., 2016b, "Identification of Infusion Strategy for Achieving Repeatable Nanoparticle Distribution and Quantifiable Thermal Dosage in Magnetic Nanoparticle Hyperthermia," *International Journal of Hyperthermia*, **32**(2):132–143.

LeCarpentier, G. L., Motamedi, M., McMath, L. P., Rastegar, S., and Welch, A. J., 1989, "The Effect of Wavelength on Ablation Mechanism During CW Laser Irradiation: Argon Verses Nd:YAG (1.32 μm)," *Proceedings of the 11th Annual IEEE Engineering in Medicine and Biology Society Conference*, pp. 1209–1210.

Lemons, D. E., Chien, S., Crawshaw, L. I., Weinbaum, S., and Jiji, L. M., 1987, "The Significance of Vessel Size and Type in Vascular Heat Transfer," *American Journal of Physiology*, **253**:R128–R135.

Li, Y., LeBrun, A., Topoleski, L. D. T., and Zhu, L., 2016, "Evaluation of Sensitivity and Accuracy of Infrared Thermography for Melanoma Screening," in *Summer Biomechanics, Bioengineering, & Biotransport Conference*, National Harbor, MD. Paper number SB3C-2016-145.

Liang, X. G., Ge, G. X., Zhang, Y. P., and Wang, G. J., 1991, "A Convenient Method of Measuring the Thermal Conductivity of Biological Tissue," *Physics in Medicine and Biology*, **36**:1599–1605.

Ling, J. X., Hand, J. W., and Young, I. R., 1999, "Effect of the SAR Distribution of a Radio Frequency (RF) Coil on the Temperature Field Within a Human Leg: Numerical Studies," ASME HTD-Vol. 363, *Advances in Heat and Mass Transfer in Biotechnology*, pp. 1–7.

Linhares, M. N., and Tasker, R. R., 2000, "Microelectrode-guided Thalamotomy for Parkinson's Disease," *Neurosurgery*, **46**:390–398.

Link, S., and El-Sayed, M. A., 2000, "Shape and Size Dependence of Radiative, Non-radiative and Photothermal Properties of Gold Nanocrystals," *Journal of International Reviews in Physical Chemistry*, **19**(3):409-453.

Liu, J., Zhu, L., and Xu, L. X., 2000, "Studies on the three-dimensional Temperature Transients in the Canine Prostate during Transurethral Microwave Thermal Therapy," *ASME Journal of Biomechanical Engineering*, **122**:372–379.

Loulou, T., and Scott, E. P., 2000, "2-D Thermal Dose Optimization in High Intensity Focused Ultrasound Treatments Using the Adjoint Method," ASME HTD-Vol. 368/BED-Vol. 47, *Advances in Heat and Mass Transfer in Biotechnology*, pp. 67–71.

Manuchehrabadi, N., Attaluri, A., Cai, H., Edziah, R., Lalanne, E., Bieberich, C., Ma, R., Johnson, A. M., and Zhu, L., 2012, "MicroCT Imaging and In Vivo Temperature Elevations in Implanted Prostatic Tumors in Laser Photothermal Therapy Using Gold Nanorods," *Journal of Nanotechnology in Engineering and Medicine*, **3**(2):021003.

Manuchehrabadi, N., Chen, Y., LeBrun, A., Ma, R., and Zhu, L., 2013a, "Computational Simulation of Temperature Elevations in Tumors Using Monte Carlo Method and Comparison to Experimental Measurements in Laser Photothermal Therapy," *Journal of Biomechanical Engineering*, **135**(12):121007.

Manuchehrabadi, N., Toughiri, R., Bieberich, C., Cai, H., Attaluri, A., Edziah, R., Lalanne, E., Johnson, A. M., Ma, R., and Zhu, L., 2013b, "Treatment Efficacy of Laser Photothermal Therapy Using Gold Nanorods," *International Journal of Biomedical Engineering and Technology,* **12**(2):157–176.

Manuchehrabadi, N., and Zhu, L., 2014, "Development of a Computational Simulation Tool to Design a Protocol for Treating Prostate Tumours Using Transurethral Laser Photothermal Therapy," *International Journal of Hyperthermia*, **30**(6):349–361.

Marion, D. W., Leonov, Y., Ginsberg, M., Katz, L. M., Kochanek, P. M., Lechleuthner, A., Nemoto, E. M., Obrist, W., Safar, P., Sterz, F., Tisherman, S. A., White, R. J., Xiao, F., and Zar, H., 1996, "Resuscitative Hypothermia," *Critical Care Medicine*, **24**(2):S81–S89.

Marion, D. W., Penrod, L. E., Kelsey, S. F., Obrist, W. D., Kochanek, P. M., Palmer, A. M., Wisniewski, S. R., and DeKosky, S. T., 1997, "Treatment of Traumatic Brain Injury with Moderate Hypothermia," *New England Journal of Medicine*, **336**:540–546.

Merello, M., Nouzeilles, M. I., Kuzis, G., Cammarota, A., Sabe, L., Betti, O., Starkstein, S., and Leiguarda, R., 1999, "Unilateral Radiofrequency Lesion versus Electrostimulation of Posteroventral Pallidum: A Prospective Randomized Comparison," *Movement Disorders*, **14**:50–56.

Mie, G., 1908, "Beiträge zur Optik Trüber Medien, Speziell Kolloidaler Metallösungen," *Annalen der Physik*, **330**(3):377–445.

Moritz, A. R., and Henriques, F. C., 1947, "Studies of Thermal Injury I: The Conduction of Heat to and through Skin and the Temperature Attained Therein: A Theoretical and an Experimental Investigation," *American Journal of Pathology*, **23**(4):530–549.

Moros, E. G., and Fan, X., 1998, "Model for Ultrasonic Heating of Chest Wall Recurrences," ASME HTD-Vol. 362/BED-Vol. 40, *Advances in Heat and Mass Transfer in Biotechnology*, pp. 27–33.

Moros, E. G., Fan, X., and Straube, W. L., 1996, "Penetration Depth Control with Dual Frequency Ultrasound," ASME HTD-Vol. 337/BED-Vol. 34, *Advances in Heat and Mass Transfer in Biotechnology*, pp. 59–65.

Matsukawa, T., Ozaki, M., Hanagata, K., Iwashita, H., Miyaji, T., and Kumazawa, T., 1996, "A Comparison of Four Infrared Tympanic Thermometers with Tympanic Membrane Temperatures Measured by Thermocouples," *Canadian Journal of Anesthesia*, **43**(12):1224–1228.

Myrhage, R., and Eriksson, E., 1984, "Arrangement of the Vascular Bed in Different Types of Skeletal Muscles,". *Progress in Applied Microcirculation*, **5**:1–14.

Myroshnychenko, V., Rodriguez-Fernandez, J., Pastoriza-Santos, I., Funston, A. M., Novo, C., Mulvaney, P., Liz-Marzan, L. M., and Garcia de Abajo, F. J., 2008, "Modeling the Optical Response of Gold Nanoparticles," *Chemical Society Reviews*, **37**(9):1792–1805.

Nadobny, J., Klopfleisch, R., Brinker, G., and Stoltenburg-Didinger, G., 2015, "Experimental Investigation and Histopathological Identification of Acute Thermal Damage in Skeletal Porcine Muscle in Relation to Whole-Body SAR, Maximum Temperature, and CEM43°C due to RF Irradiation in an MR Body Coil of Birdcage Type at 123 MHz," *International Journal of Hyperthermia*, **31**(4): 409–420.

Nakayama, A., and Kuwahara, F., 2008, "A General Bioheat Transfer Model Based on the Theory of Porous Media," *International Journal of Heat and Mass Transfer*, **51**:3190–3199.

Nath, S., DiMarco, J. P., and Haines, D. E., 1994, "Basic Aspect of Radio frequency Catheter Ablation," *Journal of Cardiovascular Electrophysiology*, **5**:863–876.

Nath, S., and Haines, D. E., 1995, "Biophysics and Pathology of Catheter Energy Delivery System," *Progress in Cardiovascular Diseases*, **37**(4):185–204.

Nussmeier, N. A., 2002, "A Review of Risk Factors for Adverse Neurological Outcome after Cardiac Surgery," *Journal of Extra-corporeal Technology*, **34**:4–10.

Obeid, A. N., Barnett, N. J., Dougherty, G., and Ward, G., 1990, "A Critical Review of Laser Doppler Flowmetry," *Journal of Medical Engineering and Technology*, **14**(5):178–181.

Oh, M. Y., Hodaie, M., Kim, S. H., Alkhani, A., Lang, A. E., and Lozano, A. M., 2001, "Deep Brain Stimulator Electrodes Used for Lesioning: Proof of Principle," *Neurosurgery*, **49**:363–369.

Ohashi, M., Matsui, T., Sekida, T., Idogawa, H., Matsugi, W., Oyama, M., Naruse, K., Kotera, Y., Yoshino, K., Ikeda, Y., and Iuchi, K., 1998, "Anti-tumor Activity of a Novel Tumor Blood Flow Inhibitor, KB-R8498," *Proceedings of the American Association for Cancer Research*, Vol. 39, pp. 312.

Overgaard, J., 1976, "Influence of Extracellular pH on the Viability and Morphology of Tumor Cells Exposed to Hyperthermia," *Journal of National Cancer Institute*, **56**:1243–1250.

Overgaard, J., 1987, "Some Problems Related to the Clinical Use of Thermal Isoeffect Doses," *International Journal of Hyperthermia*, **3**:329–336.

Parker, D. L., Smith, V., Sheldon, P., Crooks, L. E., and Fussell, L., 1982, "Temperature Distribution Measurements in Two-dimensional NMR Imaging," *Medical Physics*, **10**(3):321–325.

Parker, W. J., Jenkins, R. J., Butler, C. P., and Abbott, G. L., 1961, "Flash Method of Determining Thermal Diffusivity, Heat Capacity, and Thermal Conductivity," *Journal of Applied Physics*, **32**:1679–1684.

Patel, N. K., Heywood, P., O'Sullivan, K., McCarter, R., Love, S., and Gill, S. S., 2003, "Unilateral Subthalamotomy in the Treatment of Parkinson's Disease," *Brain*, **126**:1136–1145.

Paul, A. K., Zachariah, S., Zhu, L., and Banerjee, R. K., 2015, "Predicting Core Body Temperature during Cold Water Immersion and Exercise: Application of a Tissue-Blood Interactive Whole Body Model," *Numerical Heat Transfer*, **68**(6):598–618.

Pennes, H. H., 1948, "Analysis of Tissue and Arterial Blood Temperatures in the Resting Human Forearm," *Journal of Applied Physiology*, **1**:93–122.

Prescott, D. M., Samulski, T. V., Dewhirst, M. W., Page, R. L., Thrall, D. E., Dodge, R. K., and Oleson, J. R., 1992, "Use of Nitroprusside to Increase Tissue Temperature During Local Hyperthermia in Normal and Tumor-bearing Dogs," *International Journal of Radiation Oncology, Biology, Physics*, **23**:377–385.

Raaymakers, B. W., Crezee, J., and Lagendijk, J. J. W., 2000, "Modeling Individual Temperature Profiles from an Isolated Perfused Bovine Tongue," *Physics in Medicine and Biology,* **45**:765–780.

Rand, R. W., Snow, H. D., Elliott, D. G., and Snyder, M., 1981, "Thermomagnetic Surgery for Cancer," *Applied Biochemistry and Biotechnology.,* **6**:265–272.

Reinhold, H. S., and Endrich, B., 1986, "Tumor Microcirculation as a Target for Hyperthermia," *International Journal of Hyperthermia*, **2**:111–137.

Reith, J., Jorgensen, H. S., Pedersen, P. M., Nakayama, H., Raaschou, H. O., Jeppesen, L. L., and Olsen, T. S., 1996, "Body Temperature in Acute Stroke: Relation to Stroke Severity, Infarct Size, Mortality, and Outcome," *Lancet,* **347**:422–425.

Roemer, R. B., 1990, "Thermal Dosimetry," in *Thermal Dosimetry and Treatment Planning*, edited by M. Gaytherie, Berlin: Springer, pp. 119–214.

Rylander, M. N., Feng, Y., Zhang, Y., Bass, J., Stafford, R. J., Volgin, A., Hazle, J. D., and Diller, K. R., 2006, "Optimizing Heat Shock Protein Expression Induced by Prostate Cancer Laser Therapy through Predictive Computational Models," *Journal of Biomedical Optics*, **11**(4):041113.

Ryu, S., Brown, S. L., Kim, S. H., Khil, M. S., and Kim, J. H., 1996, "Preferential Radiosensitization of Human Prostatic Carcinoma Cells by Mild Hyperthermia," *International Journal of Radiation Oncology, Biology, Physics*, **34**(1):133–138.

Salloum, M., Ma, R., Weeks, D., and Zhu, L., 2008a, "Controlling Nanoparticle Delivery in Magnetic Nanoparticle Hyperthermia for Cancer Treatment: Experimental Study in Agarose Gel," *International Journal of Hyperthermia*, **24**(4):337–345.

Salloum, M., Ma, R., and Zhu, L., 2008b, "An In-Vivo Experimental Study of the Temperature Elevation in Animal Tissue during Magnetic Nanoparticle Hyperthermia," *International Journal of Hyperthermia*, **24**(7):589–601.

Salloum, M. D., 2005, "A New Transient Bioheat Model of the Human Body and Its Integration to Clothing Models," M.S. Thesis, American University of Beirut.

Sapareto, S. A., and Dewey, W. C., 1984, "Thermal Dose Determination in Cancer Therapy," *International Journal of Radiation Oncology, Biology, Physics,* **10**(6):787–800.

Sapozink, M. D., Cetas, T., Corry, P. M., Egger, M. J., Fessenden, P., and The NCI Hyperthermia Equipment Evaluation Contractors' Group, 1988, "Introduction to Hyperthermia Device Evaluation," *International Journal of Hyperthermia*, **4**:1–15.

Schabauer, A. M. A., and Rooke, T. W., 1994, "Cutaneous Laser Doppler Flowmetry: Applications and Findings," *Mayo Clinic Proceedings*, **69**:564–574.

Scheinman, M. M., Morady, F., Hess, D. S., and Gonzalez, R., 1982, "Catheter-induced Ablation of the Atrioventricular Junction to Control Refractory Supraventricular Arrhythmias," *JAMA*, **248**:851–855.

Shibasaki, M., Kondo, N., Tominaga, H., Aoki, K., Hasegawa, E., Idota, Y., and Moriwaki, T., 1998, "Continuous Measurement of Tympanic Temperature with a New Infrared Method Using an Optical Fiber," *Journal of Applied Physiology*, **85**(3):921–926.

Shrivastava, D., and Vaughan, J. T., 2009, "A Generic Bioheat Transfer Thermal Model for a Perfused Tissue," *Journal of Biomechanical Engineering*, **131**:074506(1–5).

Smith, C. E., 1991, "A Transient Three-Dimensional Model of the Thermal System," Ph.D. Dissertation, Kansas State University.

Smits, G. J., Roman, R. J., and Lombard, J. H., 1986, "Evaluation of Laser-Doppler Flowmetry as a Measure of Tissue Blood Flow," *Journal of Applied Physiology*, **61**(2):666–672.

Song, C. W., 1984, "Effect of Local Hyperthermia on Blood Flow and Microenvironment: A Review," *Cancer Research*, **44**:4721s–4730s.

Song, C. W., 1991, "Role of Blood Flow in Hyperthermia," in *Hyperthermia and Oncology*, M. Urano and E. B. Douple, eds., VSP Publishers, Utrecht, The Netherlands, Vol. 3, pp. 275–315.

Song, C. W., Kim, G. E., Lyons, J. C., Makepeace, C. M., Griffin, R. J., Rao, G. H., and Cragon, E. J. Jr., 1994, "Thermosensitization by Increasing Intracellular Acidity with Amiloride and its Analogs," *International Journal of Radiation Oncology, Biology, Physics*, **30**:1161–1169.

Stauffer, P. R., Rossetto, F., Leoncini, M., and Gentilli, G. B., 1998, "Radiation Patterns of Dual Concentric Conductor Microstrip Anttennas for Superficial Hyperthermia," *IEEE Transactions on Biomedical Engineering*, **45**(5):605–613.

Stoy, R. D., Foster, K. R., and Schwan, H. P., 1982, "Dielectric Properties of Mammalian Tissues from 0.1 to 100 MHz: A Summary of Recent Data," *Physics in Medicine and Biology*, **27**:501–513.

Strohbehn, J. W., 1984, "Calculation of Absorbed Power in Tissue for Various Hyperthermia Devices," *Cancer Research* (Suppl) **44**:4781s–4787s.

Su, P. C., Tseng, H-M., Liu, H-M., Yen, R-F., and Liou, H-H., 2002, "Subthalamotomy for Advanced Parkinson's Disease," *Journal of Neurosurgery*, **97**:598–606.

Thomsen, S., 1991, "Pathologic Analysis of Photothermal and Photomechanical Effects of Laser-Tissue Interactions," *Photochemistry and Photobiology*, **53**:825–835.

Torres, J. H., Motamedi, M., and Welch, A. J., 1990, "Disparate Absorption of Argon Laser Radiation by Fibrous Verses Fatty Plaque: Implications for Laser Angioplasty," *Lasers in Surgery and Medicine*, **10**:149–157.

Vesnovsky, O., Li, Y., Topoleski, L. D. T., and Zhu, L., 2017, "Modeling of Differences between Body Core and Forehead Temperatures Measured by Infrared Thermometers," *ASME 2017 Design of Medical Devices Conference*, #DMD2017-3439, April 2017, Minneapolis, MN.

Wagner, K. R., and Zuccarello, M., 2005, "Local Brain Hypothermia for Neuroprotection in Stroke Treatment and Aneurysm Repair," *Neurological Research*, **27**:238–245.

Wang, Y., and Zhu, L., 2007, "Selective Brain Hypothermia Induced by an Interstitial Cooling Device in Human Neck: Theoretical Analyses," *European Journal of Applied Physiology*, **101**(1):31–40.

Wang, Y., Zhu, L., and Rosengart, A. J., 2008, "Targeted Brain Hypothermia Induced by an Interstitial Cooling Device in the Rat Neck: Experimental Study and Model Validation," *International Journal of Heat and Mass Transfer*, **51**:5662–5670.

Wass, C. T., Lanier, W. L., Hofer, R. E., Scheithauer, B. W., and Andrews, A. G., 1995, "Temperature Changes of $\geq 1°C$ Alter Functional Neurological Outcome and Histopathology in a Canine Model of Complete Cerebral Ischemia," *Anesthesia,* **83**:325–335.

Weinbaum, S., and Jiji, L. M., 1985, "A New Simplified Bioheat Equation for the Effect of Blood Flow on Local Average Tissue Temperature," *ASME Journal of Biomechanical Engineering*, **107**:131–139.

Weinbaum, S., Jiji, L. M., and Lemons, D. E., 1984, "Theory and Experiment for the Effect of Vascular Microstructure on Surface Tissue Heat Transfer—Part I: Anatomical Foundation and Model Conceptualization," *ASME Journal of Biomechanical Engineering,* **106**:321–330.

Weinbaum, S., Xu, L. X., Zhu, L., and Ekpene, A., 1997, "A New Fundamental Bioheat Equation for Muscle Tissue: Part I—Blood Perfusion Term," *ASME Journal of Biomechanical Engineering*, **119**:278–288.

Westcott, S. L., Oldenburg, S. J., Lee, T. R., and Halas, N. J., 1998, "Formation and Adsorption of Clusters of Gold Nanoparticles onto Functionalized Silica Nanoparticle Surfaces," *Langmuir: the ACS Journal of Surfaces and Colloids*, **14**(19):5396–5401.

Whitmore, R. L., 1968, *Rheology of Circulation*, Pergamon Press, London.

Whelan, W. M., and Wyman, D. R., 1999, "A Model of Tissue Charring During Interstitial Laser Photocoagulation: Estimation of the Char Temperature," ASME HTD-Vol. 363/BED-Vol. 44, *Advances in Heat and Mass Transfer in Biotechnology*, pp. 103–107.

Wissler, E. H., 1985, "Mathematical Simulation of Human Thermal Behavior Using Whole Body Models," in *Heat and Mass Transfer in Medicine and Biology*, Chapter 13, pp. 325–373, New York: Plenum Press.

Wissler, E. H., 1998, "Pennes' 1948 Paper Revisited," *Journal of Applied Physiology*, **85**:35–41.

Wong, T. Z., Jonsson, E., Hoopes, P. J., Trembly, B. S., Heaney, J. A., Douple, E. B., and Coughlin, C. T., 1993, "A Coaxial Microwave Applicator for Transurethral Hyperthermia of the Prostate," *The Prostate*, **22**:125–138.

Wonnell, T. L., Stauffer, P. R., and Langberg, J. J., 1992, "Evaluation of Microwave and Radio Frequency Catheter Ablation in a Myocardium-equivalent Phantom Model," *IEEE Transactions on Biomedical Engineering*, **39**:1086–1095.

Xu, L. X., and Anderson, G. T., 1999, "Techniques for Measuring Blood Flow in the Microvascular Circulation," in *Biofluid Methods and Techniques in Vascular, Cardiovascular, and Pulmonary Systems*, Vol. 4, Chapter 5, Newark, NJ: Gordon and Breach Science Publisher.

Xu, L. X., Chen, M. M., Holmes, K. R., and Arkin, H., 1991, "The Theoretical Evaluation of the Pennes, the Chen-Holmes and the Weinbaum-Jiji Bioheat Transfer Models in the Pig Renal Cortex," ASME WAM, Atlanta, HTD-Vol. 189, pp. 15–22.

Xu, L. X., Chen, M. M., Holmes, K. R., and Arkin, H., 1993, "Theoretical Analysis of the Large Blood Vessel Influence on the Local Tissue Temperature Decay after Pulse Heating," *ASME Journal of Biomechanical Engineering*, **115**:175–179.

Xu, L. X., Zhu, L., and Holmes, K. R., 1998, "Thermoregulation in the Canine Prostate during Transurethral Microwave Hyperthermia, Part I: Temperature Response," *International Journal of Hyperthermia*, **14**(1):29–37.

Yavuz, M. S., Cheng, Y., Chen, J., Cobley, C. M., Zhang, Q., Rycenga, M., Xie, J., Kim, C., Song, K. H., Schwartz, A. G., Wang, L. V., and Xia, Y., 2009, "Gold Nanocages Covered by Smart Polymers for Controlled Release with Near-Infrared Light," *Nature Mater*, **8**(12):935–939.

Zhu, L., Banerjee, R. K., Salloum, M., Bachmann, A. J., and Flower, R. W., 2008, "Temperature Distribution during ICG Dye-enhanced Laser Photocoagulation of Feeder Vessels in Treatment of AMD-related Choroidal Neovascularization (CNV)," *ASME Journal of Biomechanical Engineering*, **130**(3):031010(1–10).

Zhu, L., He, Q., Xu, L. X., and Weinbaum, S., 2002, "A New Fundamental Bioheat Equation for Muscle Tissue: Part II—Temperature of SAV Vessels," *ASME Journal of Biomechanical Engineering*, **124**:121–132.

Zhu, L., Lemons, D. E., and Weinbaum, S., 1995, "A New Approach for Prediction the Enhancement in the Effective Conductivity of Perfused Muscle Tissue Due to Hyperthermia," *Annals of Biomedical Engineering*, **23**:1–12.

Zhu, L., Pang, L., and Xu, L. X., 2005, "Simultaneous Measurements of Local Tissue Temperature and Blood Perfusion Rate in the Canine Prostate during Radio Frequency Thermal Therapy," *Biomechanics and Modeling in Mechanobiology,* **4**(1):1–9.

Zhu, L., Schappeler, T., Cordero-Tumangday, C., and Rosengart, A. J., 2009a, "Thermal Interactions between Blood and Tissue: Development of a Theoretical Approach in Predicting Body Temperature during Blood Cooling/Rewarming," *Advances in Numerical Heat Transfer*, **3**:197–219.

Zhu, L., Tolba, M., Arola, D., Salloum, M., and Meza, F., 2009b, "Evaluation of Effectiveness of Er,Cr:YSGG Laser for Root Canal Disinfection: Theoretical Simulation of Temperature Elevations in Root Dentin," *Journal of Biomechanical Engineering*, **131**(7):071004(1–8).

Zhu, L., Weinbaum, S., and Lemons, D. E., 1996a, "Microvascular Thermal Equilibration in Rat Cremaster Muscle," *Annals of Biomedical Engineering*, **24**:109–123.

Zhu, L., and Xu, L. X., 1999, "Evaluation of the Effectiveness of Transurethral Radio Frequency Hyperthermia in the Canine Prostate: Temperature Distribution Analysis," *ASME Journal of Biomechanical Engineering*, **121**(6):584–590.

Zhu, L., Xu, L. X., and Chencinski, N., 1998, "Quantification of the 3-D Electromagnetic Power Absorption Rate in Tissue During Transurethral Prostatic Microwave Thermotherapy Using Heat Transfer Model," *IEEE Transactions on Biomedical Engineering*, **45**(9):1163–1172.

Zhu, L., Xu, L. X., Yuan, D. Y., and Rudie, E. N., 1996b, "Electromagnetic (EM) Quantification of the Microwave Antenna for the Transurethral Prostatic Thermotherapy," ASME HTD-Vol. 337/BED-Vol. 34, *Advances in Heat and Mass Transfer in Biotechnology*, pp. 17–20.

Zou, Y.-P., Li, W.-M., Zheng, F., Li, F.-C., Huang, H., Du, J.-D., and Liu, H.-R., 2010, "Intraoperative Radiofrequency Ablation Combined with 125 Iodine Seed Implantation for Unresectable Pancreatic Cancer," *World Journal of Gastroenterology*, **16**:5104–5110.